

Momentum tunneling between nanoscale liquid flows

Baptiste Coquinot^{1,2†}, Anna T. Bui^{3,†}, Damien Toquer¹, Angelos Michaelides³, Nikita Kavokine^{2,4,5*}, Stephen J. Cox^{3,6*} and Lydéric Bocquet^{1*a)}

¹⁾ *Laboratoire de Physique de l'École Normale Supérieure, 24 rue Lhomond, 75005, Paris,*

France

²⁾ *Max Planck Institute for Polymer Research, Ackermannweg 10, Mainz, Germany*

³⁾ *Yusuf Hamied Department of Chemistry, University of Cambridge, Cambridge CB2 1EW, United Kingdom*

⁴⁾ *Center for Computational Quantum Physics, Flatiron Institute, 162 5th Avenue, 10010 New York,*

USA

⁵⁾ *The Quantum Plumbing Lab (LNQ), École Polytechnique Fédérale de Lausanne (EPFL), Station 6, CH-1015 Lausanne, Switzerland*

⁶⁾ *Department of Chemistry, Durham University, Durham, UK*

†: *these authors contributed equally*

The world of nanoscales in fluidics is the frontier where the continuum of fluid mechanics meets the atomic, and even quantum, nature of matter. While water dynamics remain largely classical under extreme confinement, several experiments have recently reported coupling between water transport and the electronic degrees of freedom of the confining materials. This avenue prompts us to reconsider nanoscale hydrodynamic flows under the perspective of interacting excitations, akin to condensed matter frameworks. Here, using a combination of many-body theory and molecular simulations, we show that the flow of a liquid can induce the flow of another liquid behind a separating wall, at odds with the prediction of continuum hydrodynamics. We further show that the range of this “flow tunneling” can be tuned through the solid’s electronic excitations, with a maximum occurring when these are at resonance with the liquid’s charge density fluctuations. Flow tunneling is expected to play a role in global transport across nanoscale fluidic networks, such as lamellar graphene oxide or MXene membranes. It further suggests exploiting the electronic properties of the confining walls for manipulating liquids via their dielectric spectrum, beyond the nature and characteristics of individual molecules.

^{a)}Electronic mail: sjc236@cam.ac.uk, nikita.kavokine@epfl.ch, lyderic.bocquet@ens.fr

Nature does many exquisite things with water and ions at small scales. This stunning observation is a source of inspiration, and a strong motivation to explore fluidic transport in nanometric confinement. And, indeed, over the last ten years, a cabinet of curiosities of unconventional nanoscale flow properties has been unveiled in nanofluidic studies.¹⁻³ This prompted many to revisit the standard frameworks of fluid dynamics. While confining walls are merely considered as boundary conditions for hydrodynamics, they are actually ‘jiggling and wiggling’ matter, being themselves the locus of fluctuations and excitations such as phonons,⁴⁻⁶ plasmons,^{7,8} etc. In particular, while the dynamics of liquid water are essentially classical at the molecular scale—grounding our understanding of water transport in classical physics—the confining surfaces may host delocalized electrons, whose behavior should be described within quantum mechanics. Many experimental studies have now hinted at a non-trivial coupling between the classical water dynamics and the quantum dynamics of these electrons. Prominent examples include: flow-induced electronic currents,⁹⁻¹² the modification of liquid wetting by substrate metallicity,¹³ heat transfer from graphene electrons to the fluid environment,¹⁴ anomalies in hydrodynamic friction at water–carbon interfaces^{7,8,15-22} and its subtle difference with insulating materials.²³

These findings have shifted perspectives on nanoscale hydrodynamics, prompting a departure from the traditional notion that the solid only acts as a static potential for the liquid molecules, to consider instead the liquid–solid interaction at the level of collective charge density fluctuations. Specifically, polar liquids such as water carry dielectric fluctuations from their collective intermolecular motions, spanning three orders of magnitude in the terahertz (THz) frequency range of the spectrum.²⁴ For carbon-based materials such as graphene and its multilayers, the THz frequency range is where low-energy electronic surface plasmon modes lie.^{25,26} Describing water’s interaction with these fluctuations is greatly simplified if its dielectric modes are formally quantized: the corresponding elementary excitations have been dubbed “hydrons”.^{10,14} The excitation perspective for the collective water modes—inspired by many-body condensed matter physics—is at the root of the fluctuation-induced (or “quantum”) friction theory, which has successfully explained several of the phenomena mentioned above^{7,8,10,27} and therefore holds the potential to reveal and explain new physics.

Here, we show that, as water on one side of a solid wall is driven, the water’s excited hydron modes interact with collective modes in the solid substrate. As a result, a flow is induced in the water on the other side of the wall, at odds with the prediction of classical hydrodynamics. We dub this phenomenon “flow tunneling”. We develop a complete theoretical and numerical

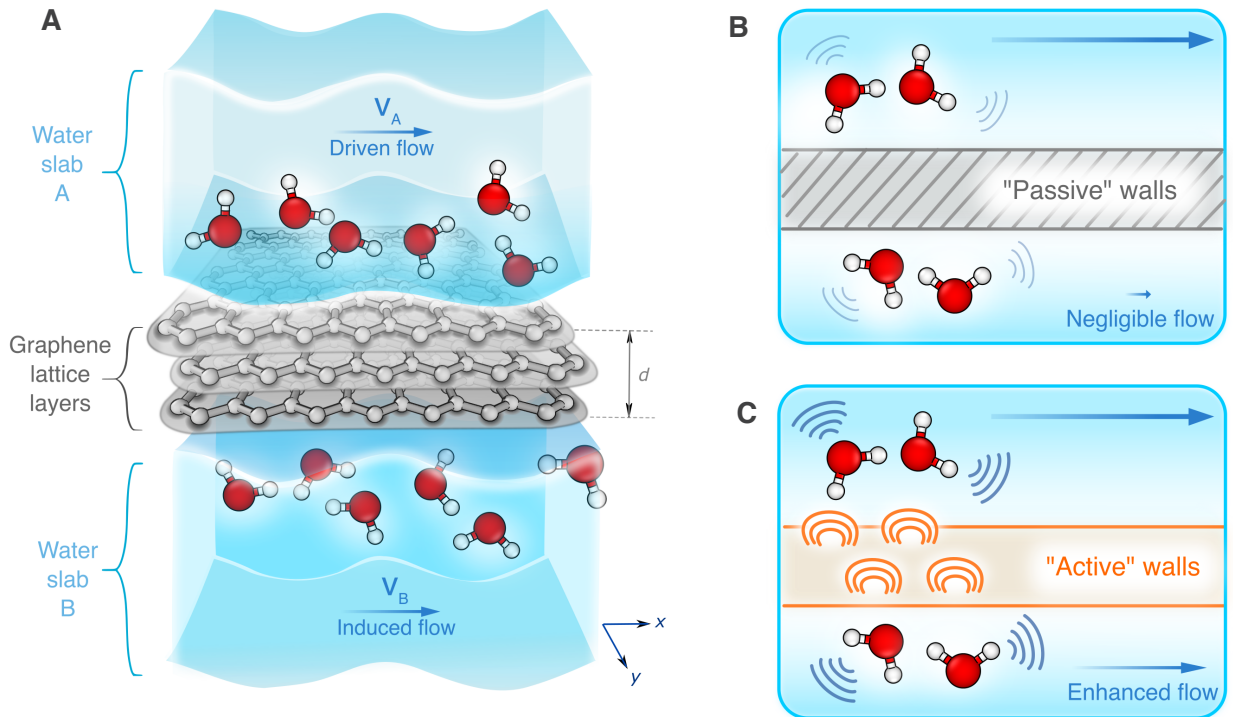


Figure 1. **Principle of flow tunneling and role of the solid wall (A)**. Schematic of the system under study. Two water slabs *A* and *B*, flowing at velocities v_A and v_B , are separated by a solid wall of thickness d . **(B)** When the wall is “passive” and only acts as a static potential, water on both sides of the solid can interact via fluctuating Coulomb forces. Direct momentum transfer between two slabs, however, is negligible so the resulting flow tunneling effect is very small. **(C)** When the wall is “active” through fluctuations in the solid coming from the electronic degrees of freedom (i.e. plasmons), the range and amplitude of flow tunneling can increase significantly due to the fluid–solid–fluid coupling.

description of flow tunneling, elucidating the role of the solid’s electronic properties in the hydron transmission process, and assessing its potential as a new principle for manipulating nanoscale liquid flows.

Flow tunneling through a passive wall

The system we consider throughout is shown schematically in Fig. 1A, and comprises a liquid water slab on one side of N two-dimensional solid layers (“fluid *A*”), with another slab of liquid water on the other side (“fluid *B*”). Before investigating the role of interactions between the solid’s and fluid’s collective modes in mediating flow tunneling, we begin with a simpler question: To what extent does a driven flow in fluid *A* directly induce a flow in fluid *B*? To this end,

we consider the case where the solid layers have no internal degrees of freedom, and interact with the fluids only via a static potential. Taking the solid layers to lie in the (x, y) plane, and assuming that fluids A and B flow with in-plane uniform velocities \mathbf{v}_A and \mathbf{v}_B , respectively, we ask whether there is a net momentum transfer (or force) from fluid A to fluid B . Such a force would originate from fluctuating Coulomb interactions between water slabs across the passive solid, and its computation in the framework of classical stochastic dynamics would be extremely involved.^{28,29} However, it can be readily estimated within an excitation perspective, using a quantum representation of the system.

The thermal charge fluctuations in each slab result in a fluctuating Coulomb potential acting on the other slab, that can be decomposed into evanescent plane waves of the form $\phi_{\mathbf{q},\omega}(\mathbf{r}, t) = \phi_0 e^{-qd} e^{i(\mathbf{q}\mathbf{r} - \omega t)}$, where \mathbf{r} lies in the (x, y) plane and d is the separation between the outermost solid layers. The elementary bosonic excitations of these modes are the hydrons, in the same way that photons are elementary excitations of the electromagnetic field; $\phi_{\mathbf{q},\omega}$ is then effectively the wavefunction of a hydron. By analogy, since the hydron wavefunctions of fluids A and B overlap, water excitations can “tunnel” between the two fluids. The hydron transmission rate is then given by the canonical Landauer formula:

$$\Gamma^{A \rightarrow B} = \frac{1}{2\pi\hbar} \sum_{\mathbf{q}} \int dE (f_{\mathbf{q}}^A(E) - f_{\mathbf{q}}^B(E)) \mathcal{T}_{\mathbf{q}}(E), \quad (1)$$

where $f_{\mathbf{q}}(E)$ is the average number of hydrons of wavevector \mathbf{q} and energy E and $\mathcal{T}_{\mathbf{q}}(E) \propto e^{-2qd}$ is the dimensionless transmission coefficient, which (as a first approximation) scales as the squared overlap of the hydron wavefunctions. If $\mathbf{v}_A = \mathbf{v}_B = 0$, $f_{\mathbf{q}}^A(E) = f_{\mathbf{q}}^B(E) = n_B(\omega = E/\hbar)$, the Bose-Einstein distribution at temperature T , and there is no net hydron transmission from A to B . Now, if $\mathbf{v}_A - \mathbf{v}_B = \Delta\mathbf{v} \neq 0$, the Bose-Einstein distributions experience a Doppler shift $\omega \mapsto \omega - \mathbf{q} \cdot \mathbf{v}_{A,B}$, so that $\Gamma^{A \rightarrow B}$ is non-vanishing. This means that there is indeed a force, or net momentum transfer from A to B , since a hydron of wavevector \mathbf{q} carries a quantum of momentum $\hbar\mathbf{q}$. To linear order in $\Delta\mathbf{v}$, and assuming a single energy scale $\hbar\omega_0 \ll k_B T$ for the hydrons, this force (per unit area) is given by

$$\begin{aligned} \frac{\mathbf{F}_{hh}}{\mathcal{A}} &\approx \frac{\omega_0}{2\pi} \frac{1}{\mathcal{A}} \sum_{\mathbf{q}} (\hbar\mathbf{q}) [n_B(\omega_0 - \mathbf{q} \cdot \Delta\mathbf{v}) - n_B(\omega_0)] e^{-2qd} \\ &\approx \frac{3k_B T}{16\pi^2 \omega_0 d^4} \Delta\mathbf{v}. \end{aligned} \quad (2)$$

F_{hh} is the driving force for the flow tunneling effect: it induces the flow of fluid B in response to the flow of fluid A . In the steady state, F_{hh} is balanced by the classical (roughness-induced)

friction $F_{\text{cl}} = -\lambda_{\text{cl}}\mathcal{A}v_{\text{B}}$ exerted on fluid B by the solid wall, so that

$$v_{\text{B}} = \frac{\lambda_{\text{hh}}}{\lambda_{\text{hh}} + \lambda_{\text{cl}}} v_{\text{A}}, \quad (3)$$

where we have defined the hydron–hydron friction coefficient as $\lambda_{\text{hh}} = F_{\text{hh}}/(\mathcal{A}\Delta v)$. The quantum formalism has enabled us to obtain a first quantitative estimate for flow tunneling with minimal computations. The final result, however, describes a purely classical effect: Planck’s constant is absent from Eq. (2). We may therefore assess the validity of our description using classical molecular dynamics (MD) simulations, where λ_{hh} is directly measured. As shown in the Supplementary Information (SI, Fig. S4), our prediction in Eq. (2) matches the simulation results at large separation d between the slabs upon setting $\omega_0 = 0.3$ THz, which is roughly the water Debye frequency. A more accurate analytical result that takes into account the full structure of the water fluctuation spectrum (SI Sec. IV) agrees with the simulation at arbitrary d .

Although qualitatively at odds with classical hydrodynamics, we find that, quantitatively, this form of flow tunneling through a passive solid is extremely short-ranged. For example, even assuming small roughness-based friction (e.g. $\lambda_{\text{cl}} \approx 2.1 \cdot 10^4 \text{ N} \cdot \text{s} \cdot \text{m}^{-3}$ for graphene), we find that v_{B} is less than 1% of v_{A} for $d \gtrsim 5 \text{ \AA}$, and thus negligible in all practical situations. We now show that the excitations of an “active” solid (Fig. 1C) drastically enhance the amplitude and range of flow tunneling, to the extent that it may become experimentally measurable.

The notion that the excitations of a solid wall can mediate momentum transfer between two liquids was in fact suggested more than 50 years ago by Andreev and Meierovich.³⁰ They considered phononic excitations, whose ability to transfer momentum is limited by the acoustic impedance mismatch between the liquid and the solid: the predicted tunneling efficiency $v_{\text{B}}/v_{\text{A}}$ is at most $\sim 10^{-5}$, whatever the solid thickness (see SI, Sec. IV C). Here, we show that the physics are very different in the case of electronic excitations, leading to tunneling efficiencies up to $v_{\text{B}}/v_{\text{A}} \sim 1$.

Molecular simulations of “active” flow tunneling

Friction forces that arise from the dynamical coupling between the electronic excitations of the solid and charge density fluctuations in the liquid are nonadiabatic in nature. Such effects are beyond the Born-Oppenheimer approximation typically employed in molecular simulations, making the prospect of modeling these with explicit electronic dynamics, on time and length scales relevant to the problem at hand, a daunting task. Recently, however, a classical molecular dynamics scheme was shown to capture the most salient aspects of fluctuation–induced quantum

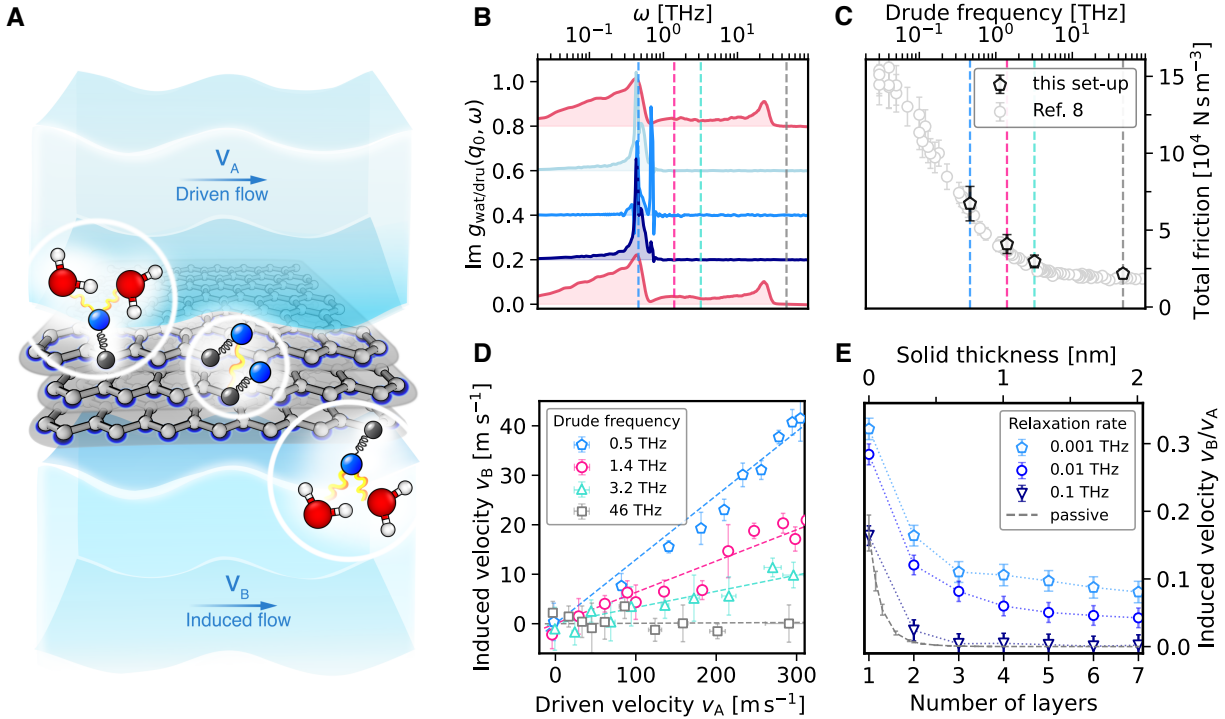


Figure 2. **Molecular simulations of flow tunneling.** **(A)** Schematic representation of system simulated with Drude oscillators, used as a classical proxy for the quantum electron dynamics. **(B)** The surface excitation spectra as measured in simulations of each component in a $N = 3$ system: water slab A, each solid layer and water slab B going from top to bottom. Here, the wavevector is $q_0 = 2.5 \text{ nm}^{-1}$ and the Drude frequency is $\omega_p = 0.5 \text{ THz}$. The vertical lines indicate the other tested frequencies for the Drude oscillators. **(C)** The total solid–liquid friction corresponding to the different Drude frequencies ω_p chosen for a system with $N = 3$, compared to result for a single water slab on a single graphene sheet in Ref. 8. The similarity of the results indicates that the friction is essentially determined by the interaction with the first solid layer. **(D)** Induced velocity through $N = 3$ layers of solid v_B versus imposed velocity v_A for the different Drude frequencies ω_p , and fixed relaxation rate $\gamma = 10^{-3} \text{ THz}$. **(E)** Tunneling efficiency v_B/v_A as a function of the number of layers N for different relaxation rates γ and fixed Drude frequency $\omega_p = 0.5 \text{ THz}$ (in blue) and through a passive solid (in gray).

friction.⁸ Here, we extend this approach to investigate “active” flow tunneling, before providing a detailed, yet more general, theoretical account.

The solid wall is modeled as a stack of N layers (with thickness $d = (N - 1)d_0$ where d_0 is the spacing between two adjacent layers), with each layer being composed of Lennard–Jones

atoms arranged in a honeycomb lattice. Electron dynamics are mimicked by giving each atom a positive charge, and attaching to it a fictitious Drude particle of equal and opposite charge via a harmonic spring (Fig. 2A).^{31,32} Relaxation processes in the solid (electron-phonon and impurity scattering, umklapp processes³³) are taken into account implicitly through an effective damping rate γ for the Drude oscillators. This gives the solid prototypical charge fluctuations described by a single plasmon-like mode at a frequency ω_p , which can be adjusted by tuning the mass of the Drude particle. While the Drude model is a crude representation for a realistic plasmon and its dispersion behavior, it allows us to capture the essential physics since its principal mode can be tuned to overlap in frequency with the water’s surface response (Fig. 2B), thereby controlling the degree of dynamical coupling between the solid and the liquid. As seen in Fig. 2C, as ω_p approaches the THz regime from above, the total solid–liquid friction increases from its “classical” surface-roughness value λ_{cl} : this extra contribution is the fluctuation-induced (quantum) friction λ_{qf} .^{7,8} Momentum transfer from the liquid to the solid is therefore enhanced by matching the frequencies of their respective charge fluctuations.

We then performed non-equilibrium molecular dynamics simulations with a pressure gradient applied to fluid *A*, and measured the resulting non-equilibrium steady state flow velocities in both fluids *A* and *B*. In the absence of Drude oscillators, no induced flow in fluid *B* could be measured for a solid thicker than a single layer, in line with our prediction in Eqs. (2) and (3). However, when the Drude frequency was set in the range of water’s Debye modes, we observed a large induced flow even through much thicker solids, up to $N = 7$ layers (Fig. 2D). For example, $v_B \approx 0.1 v_A$ for a 2 nm thick ($N = 7$) solid with $\omega_p = 0.1$ THz and relaxation rate $\gamma = 10^{-3}$ THz. The induced velocity v_B scaled linearly with the driven velocity v_A in the investigated range (Fig. 2D).

Our simulations thus reveal that the coupling to the solid’s charge fluctuation modes does not simply take momentum away from fluid *A* through friction. Momentum is in fact accumulated in those modes, and part of it is transmitted to fluid *B*, resulting in flow tunneling. The amount of momentum accumulation is sensitive to the relaxation rate γ , with faster relaxation leading to weaker flow tunneling (Fig. 2E). While in our simulations, the Drude particles themselves do not flow, in a real solid, there would be propagation of both collective plasmons and single electrons. The latter would induce an electric current parallel to the surface, akin to the Coulomb drag phenomenon.³⁴ We finally note that the momentum transfer is measured to be important in spite the fluid flow being transverse to the direction of momentum transfer across the layers,

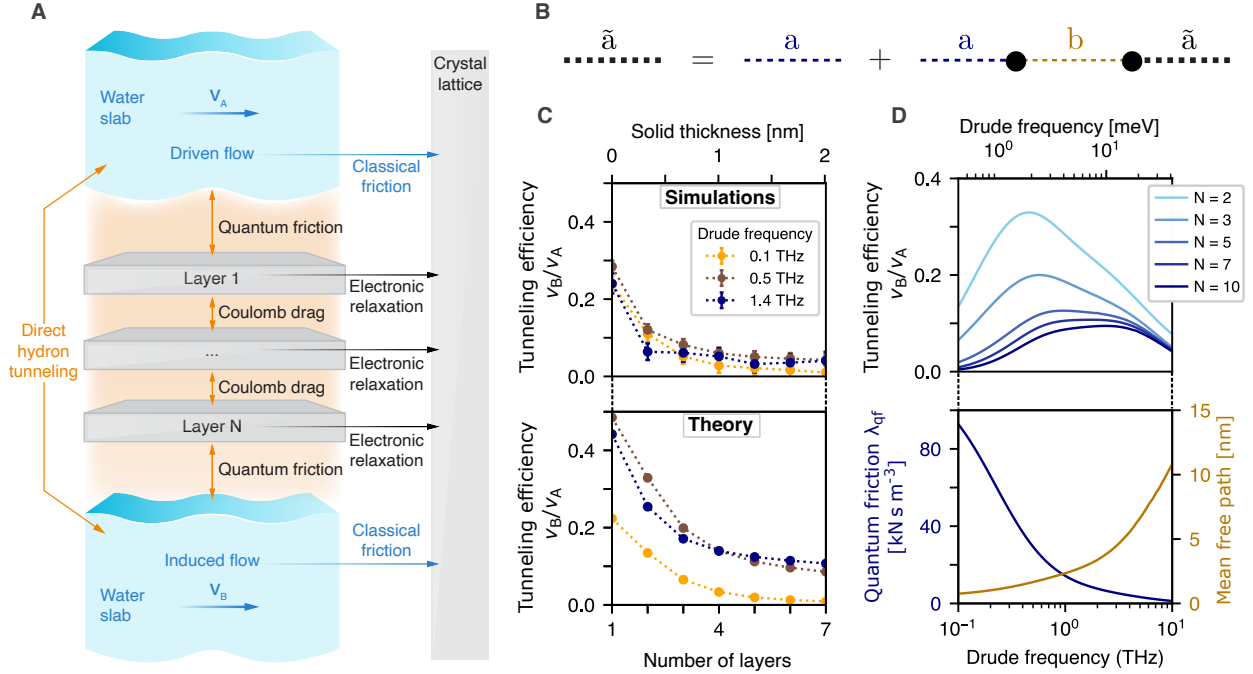


Figure 3. **Quantum theory of flow tunneling.** **(A)** Diagram representing the momentum fluxes in the liquid–solid–liquid system. Momentum can be transferred from fluid A to fluid B sequentially through the N solid layers, or through direct hydron tunneling if the solid is thin. The processes that dissipate momentum are represented by the horizontal arrows. **(B)** Dyson equation for the surface response function of layer a renormalized by the interactions with layer b . A thin line represents a bare response function (in blue for a and gold for b) while the black thick lines represent the renormalized response function of a . **(C)** Tunneling efficiency v_B/v_A as a function of the number of layers for different Drude frequencies ω_p and a relaxation rate of $\gamma = 10^{-2}$ THz. Top: simulation data. Bottom: theoretical prediction. **(D)** Tunneling efficiency v_B/v_A (top) as a function of the Drude frequency ω_p for a relaxation rate of $\gamma = 10^{-2}$ THz. There is an optimal Drude frequency because of the trade-off between the two quantities plotted at the bottom: the quantum friction coefficient (in blue) and the hydron mean free path inside the solid (in gold).

a point further confirmed by the theoretical modelling.

Many-body quantum theory of flow tunneling

Guided by the simulation results, we now develop a theory of flow tunneling through an active solid. Within our formally quantum picture, flow tunneling through a passive solid amounted

to coherent hydron transport between the two fluids – it was therefore described by a Landauer formula. The active solid now plays the role of a "junction" placed between the two hydron reservoirs (the fluids). As highlighted by the strong dependence of the simulation results on the relaxation parameter γ , the hydron transport through this junction cannot be considered coherent, and its description therefore requires going beyond the Landauer formalism. In order to account for decoherence, we model the solid by a layered structure in our simulations. The hydrons are transported coherently between the layers, but they can undergo inelastic scattering (i.e., decoherence) within each of the layers. Technically, we use the Keldysh formalism of perturbation theory, which has proven to be an asset in the study of non-equilibrium solid-liquid systems.^{7,10} Our computation is fully detailed in the SI, Sec. III-V; here, we outline the main steps.

The system is described in terms of the fluctuating charge densities $n(\mathbf{r}, t)$ of both the liquid slabs and the solid layers. It is governed by the Hamiltonian comprising all Coulomb interactions: between the water and the solid, between the two water slabs and between the different solid layers. To keep the computations tractable, we assume that a solid layer interacts only with its nearest neighbors (Fig. 3A). Our goal is to evaluate the average Coulomb force exerted by the N^{th} solid layer on the fluid slab B , in the non-equilibrium state where fluid A flows at velocity v_A :

$$\mathbf{F}_{NB} = \int d\mathbf{r}_N d\mathbf{r}_B \langle n_N(\mathbf{r}_N, t) V(\mathbf{r}_N - \mathbf{r}_B) n_B(\mathbf{r}_B, t) \rangle, \quad (4)$$

where \mathbf{r}_N and \mathbf{r}_B are the spatial coordinates in layer N and fluid slab B , respectively, and V is the Coulomb potential. To this end, we formally quantize the charge densities as free Gaussian fields – this is an approximation that amounts to neglecting interactions between excitations. The liquid and the solid are then fully characterized by their charge density correlation functions, which can be evaluated starting from the microscopic model of one's choice. In the following, we will describe the solid by the correlation function of the Drude oscillator model, to allow for direct comparison with the simulations. However, one could model each solid layer as a 2D electron gas with appropriate electron-electron and electron-phonon interactions (accounting for decoherence), so as to describe realistic solid-state systems that cannot be treated classically, such as few-layer transition metal dichalcogenides or MXenes.

The model defined in this way is in fact integrable (the Hamiltonian is quadratic in the charge densities), so that the non-equilibrium state of the system can be determined exactly using the Keldysh formalism. In practice, we perturbatively expand the average in Eq. (4) in powers of

the Coulomb interaction, and exactly resum the infinitely many terms of this expansion. The basic building blocks of the expansion are the *surface response functions* g of each of the water slabs and solid layers. These are appropriately normalized charge density correlation functions: $g(\mathbf{q}, \omega) \sim V_q \langle n_{\mathbf{q}} n_{-\mathbf{q}} \rangle_{\omega}$, where $V_q = e^2 / (2\epsilon_0 q)$ is the Fourier-transformed Coulomb potential and the $n_{\mathbf{q}}$ are charge density operators. Precise definitions of these quantities are given in the SI, Sec. III.C. In the Keldysh formalism, these correlation functions possess three components (g^R, g^A, g^K), corresponding to different time orderings of the operators. In the non-interacting equilibrium state, the Drude response function of a solid layer is

$$g_{\text{eq, Drude}}^R = \frac{\omega_p^2 f(q)}{\omega_p^2 - \omega^2 - 2i\gamma\omega}, \quad (5)$$

and the water surface response function is modeled, following Ref. 7, as a sum of two Debye peaks:

$$g_{\text{eq, Water}}^R = \sum_{i=1,2} \frac{f_i(q)}{1 - i\omega/\omega_{D,i}}. \quad (6)$$

The values of the parameters and expressions of the functions $f(q)$ are given in the SI, Sec. IV. The imposed flow in the fluid A and the induced flow in the fluid B are described, as before, by a Doppler shift in the non-equilibrium water surface response function versus its equilibrium expression: $g(\mathbf{q}, \omega) = g_{\text{eq}}(\mathbf{q}, \omega - \mathbf{q} \cdot \mathbf{v}_{A,B})$. The expansion proceeds in two steps. First, the non-equilibrium response functions of the N solid layers are determined by solving a series of Dyson equations, accounting for the inter-layer coupling via the electrostatic interactions and decoherence process throughout the solid. These equations have a very simple diagrammatic representation (Fig. 3B) – since the Hamiltonian is quadratic in the density operators – and they are algebraic in Fourier space. For example, the renormalisation of the layer $i + 1$ by the layer i for the retarded component is given by $g_{i+1}^R = g_{i+1}^{R,\text{eq}} + g_{i+1}^{R,\text{eq}} g_i^R g_{i+1}^R$, and the expression for the Keldysh component is given in the SI, Sec. III D. Then, the expansion of Eq. (4) is carried out in terms of those response functions, yielding the force acting on the B fluid across the N layers of material:

$$\frac{\mathbf{F}_{NB}}{\mathcal{A}} = \int \frac{d\mathbf{q}}{(2\pi)^2} (\hbar\mathbf{q}) (\Gamma_{NB}(\mathbf{q}) - \Gamma_{BN}(\mathbf{q})) \quad (7)$$

with

$$\Gamma_{\text{ab}}(\mathbf{q}) = \int \frac{d\omega}{4i\pi} \frac{\text{Im} [g_a^R(\mathbf{q}, \omega)] g_b^K(\mathbf{q}, \omega)}{|1 - g_a^R(\mathbf{q}, \omega) g_b^R(\mathbf{q}, \omega)|^2}. \quad (8)$$

Eqs. (7) and (8) are our main theoretical result, which has general validity beyond the particular Drude model of the solid we have considered so far. It is a far-from-equilibrium generalization of quantum friction,⁷ which echoes the Landauer formula in Eq. (1). For true interacting electrons, our result is valid at the level of a self-consistent Hartree approximation. \mathbf{F}_{NB} depends on both v_A and v_B and can be expanded to linear order in these velocities, defining two friction coefficients: $\mathbf{F}_{NB}/\mathcal{A} = \lambda_{\text{drive}}\mathbf{v}_A - \lambda_{\text{qf}}\mathbf{v}_B$. The coefficient λ_{qf} is the fluctuation-induced (quantum) friction coefficient between the fluid slab B and the N^{th} solid layer at equilibrium. The coefficient λ_{drive} accounts for the "remote drag" exerted by fluid A on fluid B – its expression is cumbersome (see SI Sec. V), but we provide in the following a scaling estimate that allows us to draw practical conclusions.

Physically, the solid gives momentum to the liquid, but then takes some of it back through quantum friction. Fluid B is also subject to an additional force due to direct hydron tunneling (λ_{hh}) if the solid is thin, and to the classical roughness-based friction (λ_{cl}) on the N^{th} layer. Momentum conservation then imposes

$$\mathbf{v}_B = \frac{\lambda_{\text{drive}} + \lambda_{\text{hh}}}{\lambda_{\text{qf}} + \lambda_{\text{cl}} + \lambda_{\text{hh}}}\mathbf{v}_A. \quad (9)$$

Eq. (9) is our theoretical prediction for the flow tunneling effect. In Fig. 3C, we compare the theoretical predictions against simulation results. Given the simplifying assumptions in the theoretical model (i.e., nearest-neighbor interactions between graphene layers, and a harmonic approximation for water's dielectric fluctuations) the agreement is remarkable, and suggests Eq. (9) captures the essential physics of the flow tunneling effect.

Conditions for optimal flow tunneling

Having established a theoretical framework, we may now assess the precise role of the solid's electronic properties in determining the range of flow tunneling. Fig. 3D shows the prediction for the tunneling efficiency v_B/v_A as a function of the Drude plasmon frequency ω_p , at fixed $\gamma = 10^{-2}$ THz. Interestingly, it exhibits a maximum at $\omega_p \sim 0.3$ THz where the Drude frequency is in resonance with the water Debye frequency (see Fig. 2B). Moreover, we observe that at small ω_p the flow tunneling efficiency decreases with increasing number of solid layers N , while at large ω_p it is nearly independent of N for $N \leq 7$.

These features can be understood if flow tunneling is represented as the transmission of discrete excitations – hydrons – between fluid A and fluid B . In Eq. (9) the friction coefficient λ_{drive} is effectively the rate at which the solid injects momentum-carrying hydrons into fluid B .

Hydrons are injected into the solid from fluid A with a rate λ_{qf} . However, they only reach fluid B if they are not scattered during their residence time τ inside the solid, which happens at a rate γ . If the solid is moderately thin, hydrons reach the opposite boundary quickly, and τ is the time it takes for a hydron to exit into fluid B : $\tau \approx \tau_{\text{sl}} \sim \lambda_{\text{qf}}^{-1}$. For thicker solids, most hydrons get scattered on their way from A to B so that $\tau \propto N$, and we may define a mean free path ℓ according to $\gamma\tau \equiv d/\ell$. Altogether (and assuming $N > 1$ so that λ_{hh} can be neglected) we obtain an asymptotic expression for the tunneling efficiency, valid for thick solids:

$$\frac{v_B}{v_A} \approx \frac{\lambda_{\text{qf}}}{\lambda_{\text{qf}} + \lambda_{\text{cl}}} e^{-(\gamma\tau_{\text{sl}} + d/\ell)}, \quad (10)$$

with τ_{sl} and ℓ both depending on the Drude frequency ω_p and relaxation rate γ . For thin solids (small N , as in our simulations), we obtain a more accurate scaling expression that accounts for the discreteness of the layers (SI Sec. V. D), but the data is still well described by Eq. (10) (Fig. S6F). Within the Drude model of the solid, λ_{qf} is a strictly decreasing function of ω_p (Fig. 3D): hydron injection into the solid is most efficient for lower Drude frequencies. However, the hydron mean free path is shorter for lower ω_p (Fig. 3D): lower frequency modes take longer to transmit their excitations to the next layer. The thicker the solid, the more flow tunneling is favored by higher plasmon frequencies. This trade-off between hydron injection rate and mean free path accounts for the 'resonant', bell-shaped dependence of the tunneling efficiency on ω_p .

Going further, the result in Eq. (10) allows us to draw general conclusions regarding the range of flow tunneling. This range is limited by the scattering rate γ of excitations inside the solid: flow can in principle tunnel through an arbitrarily thick solid if there is no dissipation inside. This is never the case in practice, and no tunneling is observed if the solid is thicker than a few times the mean free path ℓ . For $d \gtrsim \ell$, the tunneling efficiency decreases exponentially with d (see Fig. 3C at low ω_p): the hydron transport is diffusive. However, the mean free path can sometimes become very large (Fig. 3D at large ω_p). Then, it is realistic to have $d \ll \ell$, and the hydron transport becomes ballistic. The tunneling efficiency is then limited by the solid-liquid crossing time $\tau_{\text{sl}} \sim \lambda_{\text{qf}}^{-1}$: hydrons are scattered as they wait in the solid to cross into fluid B . v_B/v_A is then independent of d as seen in Fig. 3D at high Drude frequencies. But in both the diffusive and the ballistic regimes, the tunneling efficiency is ultimately determined by comparing the residence time of an excitation inside the solid to its inelastic scattering (or dephasing) rate.

We have thus identified the three qualitative determinants of flow tunneling: hydron injection rate, hydron mean free path ℓ , and hydron exit rate τ_{sl}^{-1} , which combine to predict the tunneling

efficiency in Eq. (10). We may now discuss the possibility of flow tunneling in a realistic solid-liquid system – such as two slabs of water separated by a graphene multilayer – based on these three ingredients. Within our model, the hydron injection rate is set by the quantum friction coefficient λ_{qf} . However, this ignores electron-phonon coupling in the solid and the resulting phonon drag effect,¹⁰ which effectively replaces λ_{qf} by $\sim \lambda_{\text{cl}}$ in Eq. (10). Because the electron-phonon and electron-hydron scattering rates typically have similar values,¹⁰ we further expect $\gamma\tau_{\text{sl}} \sim 1$. Therefore, the one key determinant of the tunneling efficiency is in fact the hydron mean free path, for which our theory may provide a quantitative estimate (SI Sec. V.D): in the Drude model framework, we find the phenomenological scaling $\ell \approx \ell_0 \sqrt{\omega_p/\gamma}$, with $\ell_0 = 0.26$ nm. Ignoring dispersion effects, the graphene plasmon mode may be approximately described by $\omega_p = 100$ THz and $\gamma = 0.6$ THz,³⁵ yielding $\ell \approx 4$ nm. We note that this is likely an underestimation, as it ignores electron transport perpendicular to the graphene layers. Overall, we may expect non-negligible flow tunneling through a 10 nm thick graphene wall, which can be readily obtained in nanofluidic systems using, e.g., van der Waals assembly.

Conclusions

Using a combination of many-body quantum theory and molecular simulations, we have shown that the flow of one liquid can induce the flow of another liquid through a solid wall of nanoscale thickness – a phenomenon termed ‘flow tunneling’. Classical hydrodynamics have so far been found to hold surprisingly well down to 1 nm wide channels. Our prediction implies that, in systems of multiple channels, the classical framework of hydrodynamics may qualitatively break down if the walls separating the channels are thinner than ~ 10 nm. The physical origin of this breakdown lies in the coupling of the liquid charge fluctuations to the solid wall’s electronic excitations. Beyond the fundamental importance of flow tunneling as an effect beyond hydrodynamics, this property is expected to be at play in global transport across nanoscale fluidic networks, in particular across membranes made of lamellar materials such as graphene oxides or MXenes.^{36,37} Flow tunneling is also a new and promising lever for manipulating liquids at the nanoscale via their dielectric spectrum, and not based on the nature and characteristics of individual molecules.

Acknowledgements

The authors thank Mischa Bonn for many fruitful discussions. We thank Lucy Reading-Ikkanda for help with figure preparation. We are also grateful for computational support from the UK national high

performance computing service, ARCHER2, for which access was obtained via the UKCP consortium and funded by EPSRC grant ref EP/X035891/1. **Funding:** B.C., D.T., A.M. and L.B. acknowledge support from ERC project *n-AQUA*, grant agreement 101071937. B.C. acknowledge support from the CFM foundation. A.T.B. acknowledges funding from the Oppenheimer Fund and Peterhouse College, University of Cambridge. The Flatiron Institute is a division of the Simons Foundation. S.J.C. is a Royal Society University Research Fellow (Grant No. URF\R1\211144) at the University of Cambridge. **Data availability:** The simulation data that support the findings of this study are openly available at the University of Cambridge Data Repository at <https://doi.org/10.17863/CAM.113204>. **Author contributions:** A.M., N.K., S.J.C, and L.B. conceptualized the project; B.C. carried out the theoretical analysis; A.T.B. designed and performed the molecular simulations; D.T. performed supporting analyses; B.C., A.T.B, A.M., N.K., S.J.C, and L.B. wrote the paper. **Competing interests:** The authors declare that they have no competing interests.

REFERENCES

- ¹N. R. Aluru, F. Aydin, M. Z. Bazant, D. Blankschtein, A. H. Brozena, J. P. de Souza, M. Elimelech, S. Faucher, J. T. Fourkas, V. B. Koman, M. Kuehne, H. J. Kulik, H.-K. Li, Y. Li, Z. Li, A. Majumdar, J. Martis, R. P. Misra, A. Noy, T. A. Pham, H. Qu, A. Rayabharam, M. A. Reed, C. L. Ritt, E. Schwegler, Z. Siwy, M. S. Strano, Y. Wang, Y.-C. Yao, C. Zhan, and Z. Zhang, “Fluids and electrolytes under confinement in single-digit nanopores,” [Chemical Reviews](#) **123**, 2737–2831 (2023).
- ²S. Faucher, N. Aluru, M. Z. Bazant, D. Blankschtein, A. H. Brozena, J. Cumings, J. Pedro de Souza, M. Elimelech, R. Epsztein, J. T. Fourkas, A. G. Rajan, H. J. Kulik, A. Levy, A. Majumdar, C. Martin, M. McEldrew, R. P. Misra, A. Noy, T. A. Pham, M. Reed, E. Schwegler, Z. Siwy, Y. Wang, and M. Strano, “Critical knowledge gaps in mass transport through single-digit nanopores: A review and perspective,” [The Journal of Physical Chemistry C](#) **123**, 21309–21326 (2019).
- ³L. Bocquet, “Nanofluidics coming of age,” [Nature Materials](#) **19**, 254–256 (2020).
- ⁴M. Ma, F. Grey, L. Shen, M. Urbakh, S. Wu, J. Z. Liu, Y. Liu, and Q. Zheng, “Water transport inside carbon nanotubes mediated by phonon-induced oscillating friction,” [Nature Nanotechnology](#) **10**, 692–695 (2015).
- ⁵S. Marbach, D. S. Dean, and L. Bocquet, “Transport and dispersion across wiggling nanopores,”

- [Nature Physics](#) **14**, 1108–1113 (2018).
- ⁶M. Lizée, B. Coquinot, G. Mariette, A. Siria, and L. Bocquet, “Anomalous friction of super-cooled glycerol on mica,” (2024), [arxiv:2403.18693 \[cond-mat\]](#).
- ⁷N. Kavokine, M.-L. Bocquet, and L. Bocquet, “Fluctuation-induced quantum friction in nanoscale water flows,” [Nature](#) **602**, 84–90 (2022).
- ⁸A. T. Bui, F. L. Thiemann, A. Michaelides, and S. J. Cox, “Classical quantum friction at water–carbon interfaces,” [Nano Letters](#) **23**, 580–587 (2023).
- ⁹M. Lizée, A. Marcotte, B. Coquinot, N. Kavokine, K. Sobnath, C. Barraud, A. Bhardwaj, B. Radha, A. Niguès, L. Bocquet, and A. Siria, “Strong electronic winds blowing under liquid flows on carbon surfaces,” [Phys. Rev. X](#) **13**, 011020 (2023).
- ¹⁰B. Coquinot, L. Bocquet, and N. Kavokine, “Quantum feedback at the solid-liquid interface: Flow-induced electronic current and its negative contribution to friction,” [Phys. Rev. X](#) **13**, 011019 (2023).
- ¹¹J. Rabinowitz, C. Cohen, and K. L. Shepard, “An electrically actuated, carbon-nanotube-based biomimetic ion pump,” [Nano Letters](#) **20**, 1148–1153 (2020).
- ¹²J. Yin, X. Li, J. Yu, Z. Zhang, J. Zhou, and W. Guo, “Generating electricity by moving a droplet of ionic liquid along graphene,” [Nature Nanotechnology](#) **9**, 378–383 (2014).
- ¹³J. Comtet, A. Niguès, V. Kaiser, B. Coasne, L. Bocquet, and A. Siria, “Nanoscale capillary freezing of ionic liquids confined between metallic interfaces and the role of electronic screening,” [Nature Materials](#) **16**, 634–639 (2017).
- ¹⁴X. Yu, A. Principi, K.-J. Tielrooij, M. Bonn, and N. Kavokine, “Electron cooling in graphene enhanced by plasmon–hydron resonance,” [Nature Nanotechnology](#) (2023), [10.1038/s41565-023-01421-3](#).
- ¹⁵M. Majumder, N. Chopra, R. Andrews, and B. J. Hinds, “Enhanced flow in carbon nanotubes,” [Nature](#) **438**, 44–44 (2005).
- ¹⁶J. K. Holt, H. G. Park, Y. Wang, M. Stadermann, A. B. Artyukhin, C. P. Grigoropoulos, A. Noy, and O. Bakajin, “Fast mass transport through sub-2-nanometer carbon nanotubes,” [Science](#) **312**, 1034–1037 (2006).
- ¹⁷A. Maali, T. Cohen-Bouhacina, and H. Kellay, “Measurement of the slip length of water flow on graphite surface,” [Applied Physics Letters](#) **92**, 053101 (2008).
- ¹⁸M. Ma, F. Grey, L. Shen, M. Urbakh, S. Wu, J. Z. Liu, Y. Liu, and Q. Zheng, “Water transport inside carbon nanotubes mediated by phonon-induced oscillating friction,” [Nature](#)

- nanotechnology **10**, 692–695 (2015).
- ¹⁹E. Secchi, S. Marbach, A. Niguès, D. Stein, A. Siria, and L. Bocquet, “Massive radius-dependent flow slippage in carbon nanotubes,” *Nature* **537**, 210–213 (2016).
- ²⁰Q. Xie, M. A. Alibakhshi, S. Jiao, Z. Xu, M. Hempel, J. Kong, H. G. Park, and C. Duan, “Fast water transport in graphene nanofluidic channels,” *Nature Nanotechnology* **13**, 238–245 (2018).
- ²¹A. Keerthi, S. Goutham, Y. You, P. Iamprasertkun, R. A. W. Dryfe, A. K. Geim, and B. Radha, “Water friction in nanofluidic channels made from two-dimensional crystals,” *Nature Communications* **12**, 3092 (2021).
- ²²B. Coquinot, M. Becker, R. R. Netz, L. Bocquet, and N. Kavokine, “Collective modes and quantum effects in two-dimensional nanofluidic channels,” *Faraday Discussions* (2023), [10.1039/D3FD00115F](https://doi.org/10.1039/D3FD00115F).
- ²³G. Tocci, L. Joly, and A. Michaelides, “Friction of water on graphene and hexagonal boron nitride from ab initio methods: Very different slippage despite very similar interface structures,” *Nano Letters* **14**, 6872–6877 (2014).
- ²⁴M. Heyden, J. Sun, S. Funkner, G. Mathias, H. Forbert, M. Havenith, and D. Marx, “Dissecting the THz spectrum of liquid water from first principles via correlations in time and space,” *Proceedings of the National Academy of Sciences* **107**, 12068–12073 (2010).
- ²⁵H. A. Hafez, S. Kovalev, J.-C. Deinert, Z. Mics, B. Green, N. Awari, M. Chen, S. German-skiy, U. Lehnert, J. Teichert, Z. Wang, K.-J. Tielrooij, Z. Liu, Z. Chen, A. Narita, K. Müllen, M. Bonn, M. Gensch, and D. Turchinovich, “Extremely efficient terahertz high-harmonic generation in graphene by hot dirac fermions,” *Nature* **561**, 507–511 (2018).
- ²⁶L. Ju, B. Geng, J. Horng, C. Girit, M. Martin, Z. Hao, H. A. Bechtel, X. Liang, A. Zettl, Y. R. Shen, and F. Wang, “Graphene plasmonics for tunable terahertz metamaterials,” *Nature Nanotechnology* **6**, 630–634 (2011).
- ²⁷B. Coquinot, L. Bocquet, and N. Kavokine, “Hydroelectric energy conversion of waste flows through hydro-electronic drag,” (2024), [arxiv:2403.20209 \[cond-mat, physics:physics\]](https://arxiv.org/abs/2403.20209).
- ²⁸D. S. Dean and A. Gopinathan, “Out-of-equilibrium behavior of Casimir-type fluctuation-induced forces for free classical fields,” *Physical Review E* **81**, 041126 (2010).
- ²⁹W. Chen, A. V. Andreev, and A. Levchenko, “Boltzmann-Langevin theory of Coulomb drag,” *Physical Review B* **91**, 245405 (2015).
- ³⁰A. F. Andreev and A. E. Meierovich, “Dragging of a liquid by a liquid through a stationary

- solid wall," *JETP Lett.* **15** (1971).
- ³¹G. Lamoureux and B. Roux, "Modeling induced polarization with classical Drude oscillators: Theory and molecular dynamics simulation algorithm," *The Journal of Chemical Physics* **119**, 3025–3039 (2003).
- ³²R. P. Misra and D. Blankschtein, "Insights on the role of many-body polarization effects in the wetting of graphitic surfaces by water," *The Journal of Physical Chemistry C* **121**, 28166–28179 (2017).
- ³³C. Kittel, *Introduction to Solid State Physics* (Wiley, 2004).
- ³⁴B. N. Narozhny and A. Levchenko, "Coulomb drag," *Rev. Mod. Phys.* **88**, 025003 (2016).
- ³⁵G. X. Ni, A. S. McLeod, Z. Sun, L. Wang, L. Xiong, K. W. Post, S. S. Sunku, B.-Y. Jiang, J. Hone, C. R. Dean, M. M. Fogler, and D. N. Basov, "Fundamental limits to graphene plasmonics," *Nature* **557**, 530–533 (2018).
- ³⁶W. Ouyang, O. Hod, and M. Urbakh, "Parity-dependent moiré superlattices in graphene/bn heterostructures: A route to mechanomutable metamaterials," *Physical Review Letters* **126**, 216101 (2021).
- ³⁷Y. Gogotsi and B. Anasori, "The Rise of MXenes," *ACS Nano* **13**, 8491–8494 (2019).

Supplementary Information
Momentum tunneling between nanoscale liquid flows

Baptiste Coquinot^{1,2†}, Anna T. Bui^{3,†}, Damien Toquer¹, Angelos
Michaelides³, Nikita Kavokine^{2,4*}, Stephen J. Cox^{3*} and Lydéric Bocquet^{1*}

¹*Laboratoire de Physique de l'Ecole Normale Supérieure, 24 rue Lhomond, 75005, Paris, France*

²*Max Planck Institute for Polymer Research, Ackermannweg 10, Mainz, Germany*

³ *Yusuf Hamied Department of Chemistry, University of Cambridge, Cambridge CB21EW, United Kingdom and*

⁴*Center for Computational Quantum Physics, Flatiron Institute,
162 5th Avenue, New York, NY 10010, USA*

†: *these authors contributed equally*

arXiv:2501.01253v1 [cond-mat.mes-hall] 2 Jan 2025

* sjc236@cam.ac.uk, nikita.kavokine@mpip-mainz.mpg.de, lyderic.bocquet@ens.fr

CONTENTS

I. Simulations with passive walls	2
A. Set-up	2
B. Simulation details	3
C. Computation of the hydron–hydron friction coefficient	3
II. Simulations of flow tunneling	4
A. Set-up	4
B. Equilibrium simulation details	5
C. Computation of surface response functions and friction coefficients	5
D. Non-equilibrium simulation details	6
III. Theoretical setup	6
A. Model	6
B. Linear response theory	6
C. Keldysh formalism	9
D. Dyson equation	10
E. Out-of-equilibrium friction forces	10
IV. Models of water and solid	11
A. Water surface response function and hydrons	11
B. Drude model of solid	11
C. Effect of phonons	12
V. Flow tunneling	13
A. Simplified expression of fluctuation-induced friction	13
B. Flow tunneling through a passive solid	13
C. Flow tunneling through an active solid	15
D. Scaling regimes of the tunneling efficiency	16
References	16

I. SIMULATIONS WITH PASSIVE WALLS

A. Set-up

For simulations with passive solid walls, we consider the system in Fig. 1A with two water slabs, each with 517 water molecules (thickness ~ 2.5 nm) separated by a passive solid of thickness d in the z direction. The top solid surface interacts with water slab A through a Lennard–Jones 9-3 potential

$$u_{\text{hi}}(z) = \epsilon_{\text{wall}} \left[\frac{2}{15} \left(\frac{\sigma_{\text{wall}}}{|z - z_{\text{hi}}|} \right)^9 - \left(\frac{\sigma_{\text{wall}}}{|z - z_{\text{hi}}|} \right)^3 \right] \quad z > z_{\text{hi}}, \quad (1)$$

and the bottom surface with water slab B through

$$u_{\text{lo}}(z) = \epsilon_{\text{wall}} \left[\frac{2}{15} \left(\frac{\sigma_{\text{wall}}}{|z - z_{\text{lo}}|} \right)^9 - \left(\frac{\sigma_{\text{wall}}}{|z - z_{\text{lo}}|} \right)^3 \right] \quad z < z_{\text{lo}}, \quad (2)$$

where $z_{\text{hi}} = z_{\text{lo}} + d$, ϵ_{wall} is the interaction strength and σ_{wall} is the interaction range. We choose $\epsilon_{\text{wall}} = 1.3 \text{ kcal mol}^{-1}$ and $\sigma_{\text{wall}} = 3.19 \text{ \AA}$, which gave a similar water density profile at the liquid–solid interface (Fig. 1B) as the water–carbon interface of Ref. [1]. However, the conclusion does not change when these parameters deviate from the quoted values.

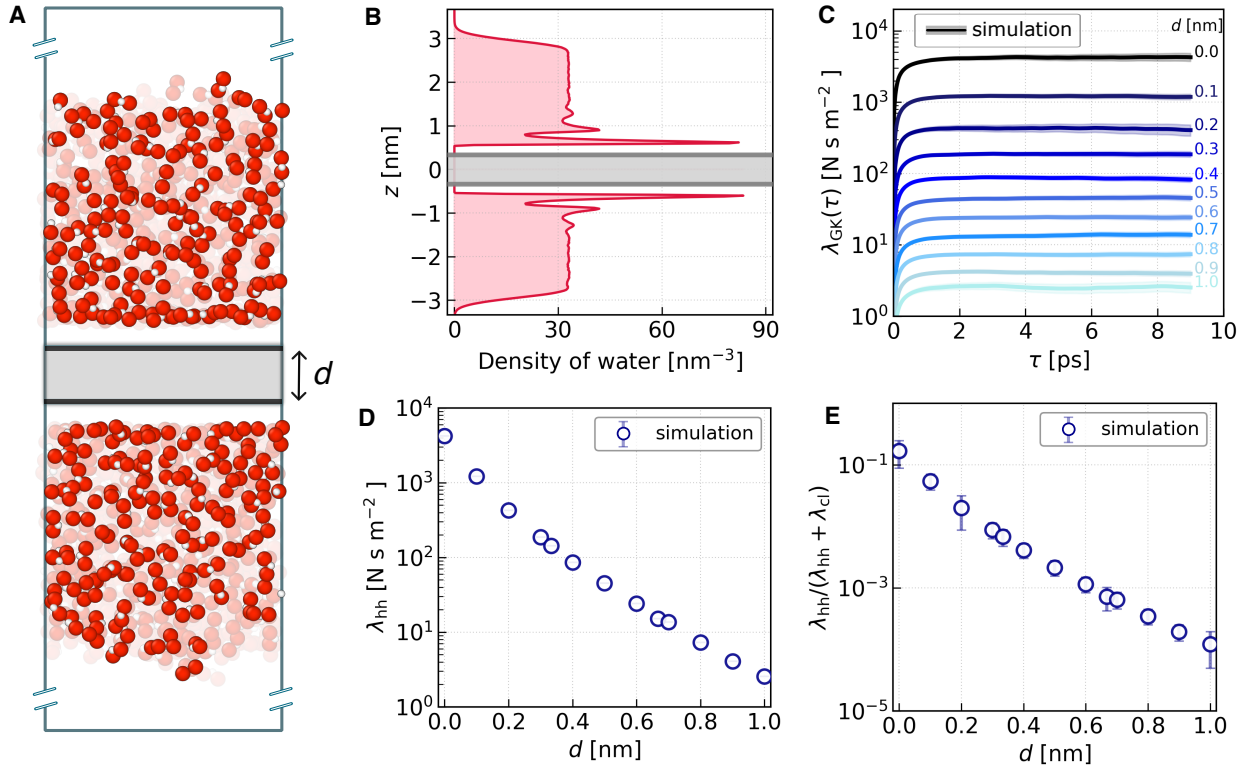


Figure 1. **Simulations with passive walls.** (A) The view from the side of the simulation set-up. Oxygen and hydrogen atoms are in red and white respectively. (B) The planar density profile of the water slabs. (C) The Green–Kubo friction integrals $\lambda_{\text{GK}}(\tau)$ for different values of thickness d . (D) The hydron–hydron friction coefficient λ_{hh} as a function of d . (E) The flow tunneling efficiency when the walls are passive calculated from Eq. 5.

B. Simulation details

Simulations were carried out with the LAMMPS simulations package [2]. The orthorhombic cell has dimension $\approx 26 \times 25 \times 300 \text{ \AA}^3$. Water–water interactions were described with the SPC/E water model [3]. The geometry of water molecules was constrained using the RATTLE algorithm [4]. All Lennard-Jones interactions were truncated and shifted at 10 \AA . Electrostatic interactions were cut off at 10 \AA and long-ranged interactions were evaluated using particle–particle particle–mesh Ewald summation [5] such that the RMS error in the forces was a factor of 10^5 smaller than the force between two unit charges separated by a distance of 1.0 \AA [6]. The Yeh–Berkowitz correction [7] was used to decouple the electrostatic interactions between the whole system and its periodic images.

The simulations were carried out in the canonical (NVT) ensemble for different d values, where the temperature was held at 300 K . Two separate Nosé–Hoover thermostats [8, 9] were applied to each water slab. Each thermostat is a Nosé–Hoover chain with 10 thermostats and a damping constant of 0.1 ps . Dynamics were propagated using the velocity Verlet algorithm with a time-step of 1 fs . Each system was equilibrated for 100 ps and the subsequent 10 ns was used for analysis to give the results presented.

C. Computation of the hydron–hydron friction coefficient

For each equilibrium MD simulation, the friction coefficient was evaluated through the Green–Kubo formula [10] involving the time integral of the force autocorrelation function

$$\lambda_{\text{GK}}(\tau) = \frac{1}{\mathcal{A}k_{\text{B}}T} \int_0^\tau dt \langle F(0) \cdot F(t) \rangle, \quad (3)$$

where \mathcal{A} is the interfacial lateral area, $\langle \dots \rangle$ indicates an ensemble average and $F(t)$ denotes the instantaneous lateral force exerted on the liquid by the solid at time t . $F(t)$ is evaluated as the total summed force acting on all water molecules of a

given configuration averaged over both in-plane dimensions (x, y) and is saved at every time-step (1 fs). In principle, the hydron–hydron friction coefficient is recovered at the long-time limit

$$\lambda_{\text{hh}} = \lim_{\tau \rightarrow \infty} \lambda_{\text{GK}}(\tau). \quad (4)$$

However, at long times, the integral in Eq. 3 decays to zero due to the finite lateral extent of the system [11, 12] so we evaluated $\lambda_{\text{GK}}(\tau)$ to a plateau as is commonly done [13–15] (see Fig. 1C). The error bars correspond to the statistical errors obtained from splitting the entire trajectory into 100 blocks such that each block is 100 ps long.

The hydron–hydron friction coefficient λ_{hh} from the simulations is shown as a function of the solid thickness d in Fig. 1D. By assuming a surface roughness-based classical friction of $\lambda_{\text{cl}} \approx 2.2 \times 10^4 \text{ N s m}^{-3}$ (justified in a later section with simulations with explicit carbon atoms) and using Eq. 3 in the main text

$$v_{\text{B}} = \frac{\lambda_{\text{hh}}}{\lambda_{\text{hh}} + \lambda_{\text{cl}}} v_{\text{A}}, \quad (5)$$

we show the prediction from simulations for the flow tunneling efficiency $v_{\text{B}}/v_{\text{A}}$ in Fig. 1E. The scaling relation between $v_{\text{B}}/v_{\text{A}}$ and d will be compared with the theory in a later section.

II. SIMULATIONS OF FLOW TUNNELING

A. Set-up

To explore the flow-tunneling effect when the solid's charge density fluctuations can play an active role, we consider a system of N solid layers sandwiched between two films of water as shown in Fig. 2A. The layers are modeled with the lattice

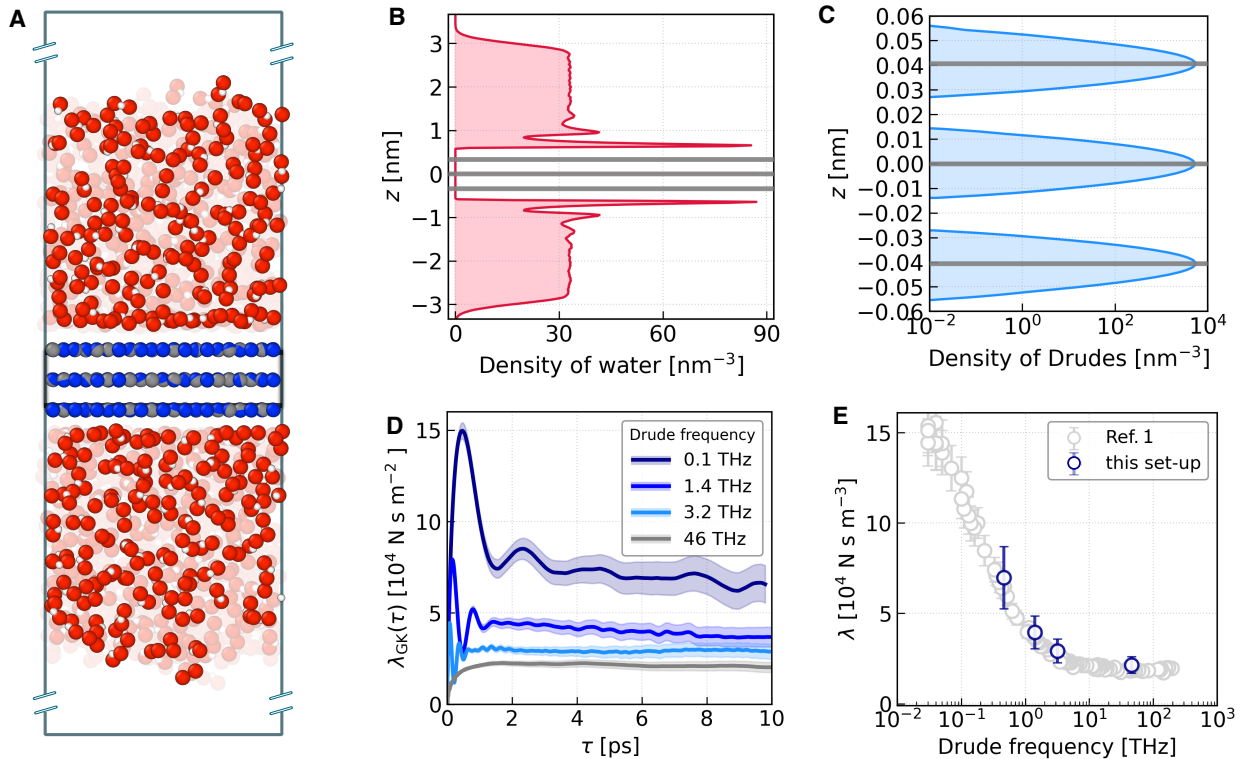


Figure 2. **Simulations with active walls with three layers of graphene.** (A) The view from the side of the simulation set-up. Oxygen, hydrogen, carbon atoms and Drude particles are in red, white, grey and blue, respectively (B) The planar density profile of the water slabs (grey lines indicate location of the graphene sheets). (C) The planar density of the Drude particles about each graphene layer. The origins for the top and bottom layers are shifted to show both three distributions on the same plot. (D) The Green–Kubo friction integrals $\lambda_{\text{GK}}(\tau)$ for different values of Drude frequencies ω_{p} . (E) The liquid–solid friction coefficient on water slab A, λ , as a function of the Drude frequency ω_{p} . Results for friction of one water slab on a single graphene layer from Ref. 1 is also shown.

and Lennard-Jones parameters of graphene. Water is modelled with the SPC/E model [3] and the water–carbon interaction is described with a 12-6 Lennard-Jones potential with the Werder parameters [16]. The dielectric response of the solid is described with the classical Drude model [17]: each C atom carries a charge $+Q_D$ and is attached to a Drude particle of mass m_D and charge $-Q_D$ with a harmonic spring with force constant k_D . Following Ref. 1, we set $Q_D = 1.852e$ and $k_D = 4184 \text{ kJ mol}^{-1} \text{ \AA}^{-2}$, which have been shown to recover the polarizability tensor of a periodic graphene lattice [18]. The resulting water density profile and distribution of Drude particles about their core carbon atoms are shown in Fig. 2B and Fig. 2C respectively. As done in Ref. 1, we treat m_D as a free parameter that tunes the frequency of each individual oscillator, which in turn controls the frequency of the single plasmon-like mode ω_p . The masses we have used and their resulting values for ω_p are given in Table 1.

Mass m_D [amu]	Drude frequency ω_p [THz]
5	46
1000	3.2
5000	1.4
50000	0.5
500000	0.1

Table 1. **Parameters for masses in simulations.** The frequencies are extracted from the location of the principal peak in the solid layers' surface response functions.

B. Equilibrium simulation details

Simulations were carried out with the LAMMPS simulations package [2]. The orthorhombic cell has dimension $\approx 26 \times 25 \times 300 \text{ \AA}^3$. Water–water interactions were described with the SPC/E water model [3]. The geometry of water molecules was constrained using the RATTLE algorithm [4]. The carbon positions of the sheet were fixed. Water–carbon interaction was modeled with Werder parameters [16]. The classical Drude oscillator model [17, 19] was employed for the polarisability of the carbon with Thole damping [20] using parameters from Misra and Blankschtein [18]. All Lennard-Jones interactions were truncated and shifted at 10 \AA . Electrostatic interactions in real space were cut off at 10 \AA and long-ranged interactions were evaluated using particle–particle particle–mesh Ewald summation [5] such that the RMS error in the forces was a factor of 10^5 smaller than the force between two unit charges separated by a distance of 1.0 \AA [6].

The simulations were carried out in the canonical (NVT) ensemble, where the temperature was held at 300 K. Two separate Nosé–Hoover thermostats [8, 9] were applied to each water slab, each being a Nosé–Hoover chain with 10 thermostats and a damping constant of 0.1 ps. The Langevin thermostat was used to control the dissipation of the Drudes particles in the solid, with a relaxation rate of γ , giving a random force $f_{\text{ran}} \propto \sqrt{k_B T m_D \gamma}$. Dynamics were propagated using the velocity Verlet algorithm with a time-step of 1 fs, unless specified otherwise. Each system was equilibrated for 100 ps and the subsequent 10 ns was used for analysis to give the results presented in the main article.

C. Computation of surface response functions and friction coefficients

We characterise the charge density distributions of the solid and the liquid by their surface response functions defined as

$$\text{Im } g(q, \omega) = \frac{\pi\omega}{q\mathcal{A}k_B T} \int_{-\infty}^{\infty} dt e^{i\omega t} \sum_{\alpha, \beta} \langle Q_\alpha Q_\beta e^{-i\mathbf{q} \cdot [\mathbf{x}_\alpha(t) - \mathbf{x}_\beta(0)]} e^{-q|z_\alpha(t) - z_0|} e^{-q|z_\beta(0) - z_0|} \rangle. \quad (6)$$

Here, Q_α is the charge on atom α , whose in-plane position at time t is $\mathbf{x}_\alpha(t)$, \mathbf{q} is a wavevector parallel to the graphene sheet, $z_\alpha(t)$ is the vertical coordinate and z_0 is a plane 1.6 \AA away from the edge of the water slab or solid surface. In practice, we computed at every time-step (1 fs) the Fourier–Laplace surface components of the charge densities for each water slab and each solid layer

$$\tilde{n}(q, t) = \sum_{\alpha} Q_\alpha e^{i\mathbf{q} \cdot \mathbf{x}_\alpha(t)} e^{-q|z_\alpha(t) - z_0|}. \quad (7)$$

As we are interested in the long-wavelength limit ($q \rightarrow 0$), we focus on $\mathbf{q} = \mathbf{q}_0$, the lowest wavevector in the x direction accessible in our simulation box, the magnitude of which is $q_0 = 2\pi/L_x \approx 0.25 \text{ \AA}^{-1}$ where L_x is the length of the box in the x direction. The power spectra of the surface charge densities are given as

$$S(q, \omega) = \frac{1}{\mathcal{A}} \int_{-\infty}^{+\infty} dt \langle \tilde{n}(q, 0) \tilde{n}(-q, t) \rangle e^{i\omega t}. \quad (8)$$

Through the fluctuation-dissipation theorem, we can obtain the imaginary part of the surface response function through

$$\text{Im} g(q, \omega) = \frac{2\pi}{q} \frac{\omega}{2k_{\text{B}}T} S(q, \omega). \quad (9)$$

To ensure the spectrum is independent of noise, a Savitzky–Golay filter [21] was applied. The resulting spectra without further fitting are presented in the main article.

The liquid–solid friction coefficient is computed via the Green–Kubo relation in analogous manner to the previous section. For a system with $N = 3$, we show the Green–Kubo integral λ_{GK} in Fig. 2D and the corresponding total friction coefficient λ in Fig. 2E. Since in our simulations, changing m_{D} does not affect static equilibrium properties such as surface roughness, we can extract the surface-roughness classical friction contribution $\lambda_{\text{cl}} \approx 2.2 \times 10^4 \text{ N s m}^{-3}$ on the water slab A from the simulations with $\omega_{\text{p}} > 20 \text{ THz}$. This is only marginally higher than $\lambda_{\text{cl}} \approx 1.9 \times 10^4 \text{ N s m}^{-3}$ estimated in Ref. 1 for a single water slab on a single graphene sheet, with the difference coming from the presence of two extra graphene layers and water slab B underneath.

D. Non-equilibrium simulation details

Non-equilibrium molecular dynamics (NEMD) simulations are carried out to study pressure-driven flow. To drive the flow of the top water film, we applied an external force on the O atom of each water molecules in the x direction while keeping the walls immobile, which generated a Poiseuille flow. The thermostats are applied only after excluding the center-of-mass contribution with a damping time of 100 fs.

To compute the flow-tunneling efficiency for a set-up with a particular number of graphene layers N , relaxation rate γ and Drude frequency ω_{p} , at least ten different simulations were run with different magnitudes of the external force. The corresponding friction force ranges up to $F/\mathcal{A} \sim 25 \times 10^5 \text{ N m}^{-2}$ for simulations with $m_{\text{D}} = 5 \text{ amu}$ and to $F/\mathcal{A} \sim 500 \times 10^5 \text{ N m}^{-2}$ for simulations with $m_{\text{D}} = 500000 \text{ amu}$. After at least 1 ns of equilibration, the velocity of both water slabs are computed by averaging over $\sim 10 \text{ ns}$ of production run. A linear regression line is fitted to the induced velocity v_{B} as function to the driven velocity v_{A} using least-squares fitting. The ratio $v_{\text{B}}/v_{\text{A}}$ is given as the slope of this regression line, with the error given as the standard error of the slope. The results for a subset of simulations are shown in Fig. 3.

III. THEORETICAL SETUP

A. Model

We consider two slabs of water, A and B, filling two half-spaces separated by N two-dimensional solid layers, as pictured in Fig. 4A. These layers are assumed translationally invariant in the (x, y) plane. We denote n_i the charge density in the i -th layer, with $i = 0 = \text{A}$ being the first water slab and $i = N + 1 = \text{B}$ the second water slab. Each layer is neutral, thus $\langle n_i \rangle = 0$. However, there can be fluctuations of charges.

Each layer is described by a Hamiltonian \mathcal{H}_i which takes into account the internal structure. In addition, the charges interact electrically both inside a layer and between layers. These interactions are of the form:

$$\mathcal{H}_{ij}(t) = \int d\mathbf{r} d\mathbf{r}' n_i(\mathbf{r}, t) V(\mathbf{r} - \mathbf{r}') n_j(\mathbf{r}', t) \quad (10)$$

where $V(\mathbf{r}) = e^2/(4\pi\epsilon_0 r)$ is the Coulomb potential. In the following we treat the inter-layer electric interactions as a perturbation. We consider interactions only between nearest-neighbor layers.

B. Linear response theory

In the perturbative framework, we will be interested by the response of a layer to the electric potential of another layer. Let us consider fluctuation $\delta n_i(\mathbf{r}, t)$ of the charge density in the layer i . This fluctuation generates an electric potential

$$\delta\phi_i(\mathbf{r}, t) = \int d\mathbf{r}' V(\mathbf{r} - \mathbf{r}') \delta n_i(\mathbf{r}', t) \quad (11)$$

The charge density induced in layer j in response to this potential is, within linear response theory:

$$\delta n_j(\mathbf{r}, t) = \int_{-\infty}^t dt' \langle [n_j(\mathbf{r}, t), \mathcal{H}_{ij}(t')] \rangle = \int_{-\infty}^t dt' \int d\mathbf{r}' d\mathbf{r}'' \langle [n_j(\mathbf{r}, t), n_j(\mathbf{r}', t')] \rangle V(\mathbf{r}' - \mathbf{r}'') \delta n_i(\mathbf{r}'', t'). \quad (12)$$

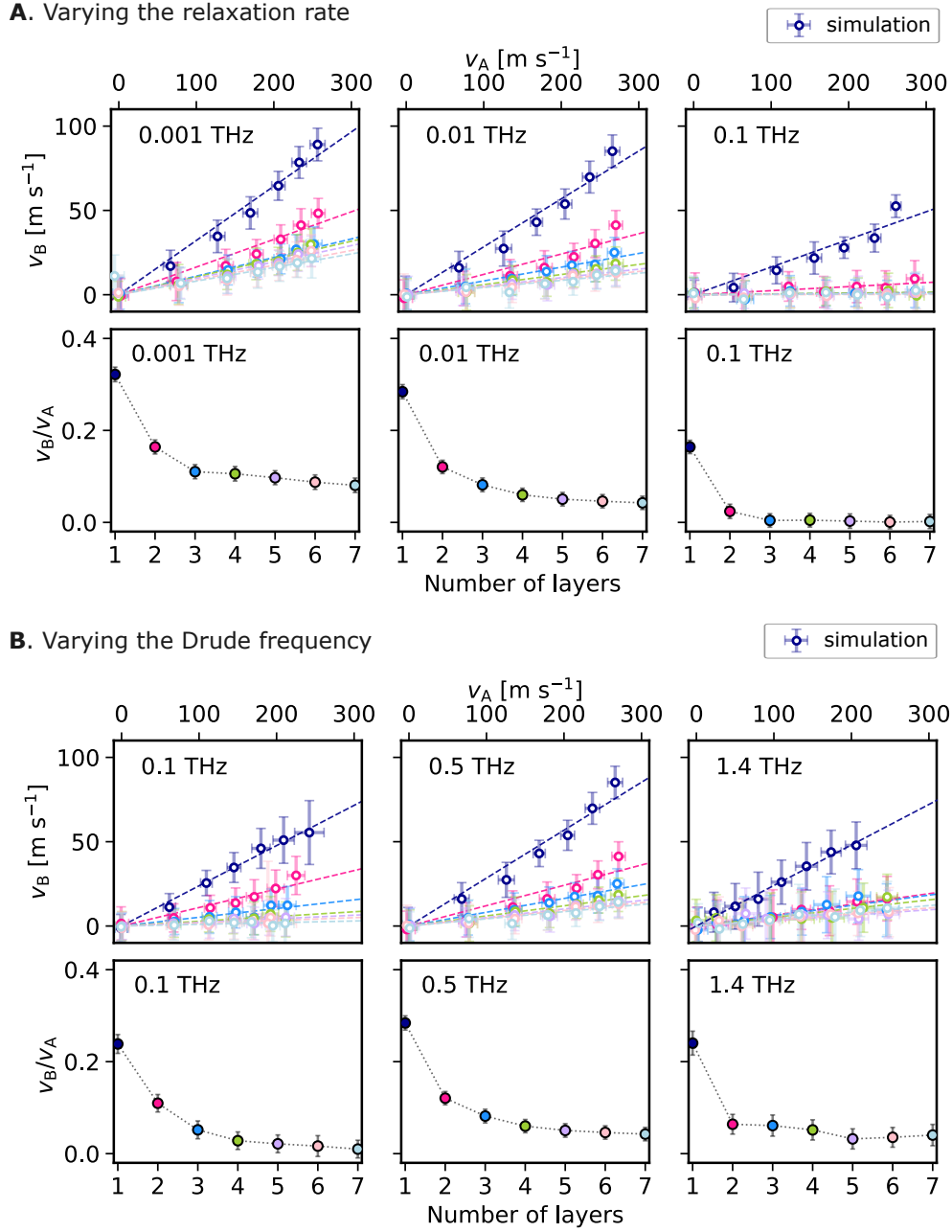


Figure 3. **Flow tunneling efficiency from non-equilibrium simulations with active walls.** **(A)** Results for different relaxation rates of the Drude particles' dissipation γ (as indicated in the left corner of each plot) for a Drude frequency of $\omega_p = 0.5$ THz. The different colors on the top line correspond to the different number of layers as represented on the bottom line. The values in the bottom panel correspond to the gradient of the fitted (dashed) curves in the top panel. **(B)** Results for different Drude frequencies ω_p (as indicated in the left corner of each plot) for a relaxation rate of $\gamma = 0.01$ THz. The different colors in the top panel correspond to the different number of layers as represented on the bottom panel. The values in the bottom panel correspond to the gradient of the fitted (dashed) curves in the top panel.

In order to simplify these convolutions, we define a transformed charge density:

$$\bar{n}_i(\mathbf{q}, t) = \sqrt{\frac{e^2}{2\epsilon_0 q}} \int d\mathbf{r} n_i(\mathbf{r}, t) e^{-i\mathbf{q}\cdot\mathbf{r} - q|\Delta z|} \quad (13)$$

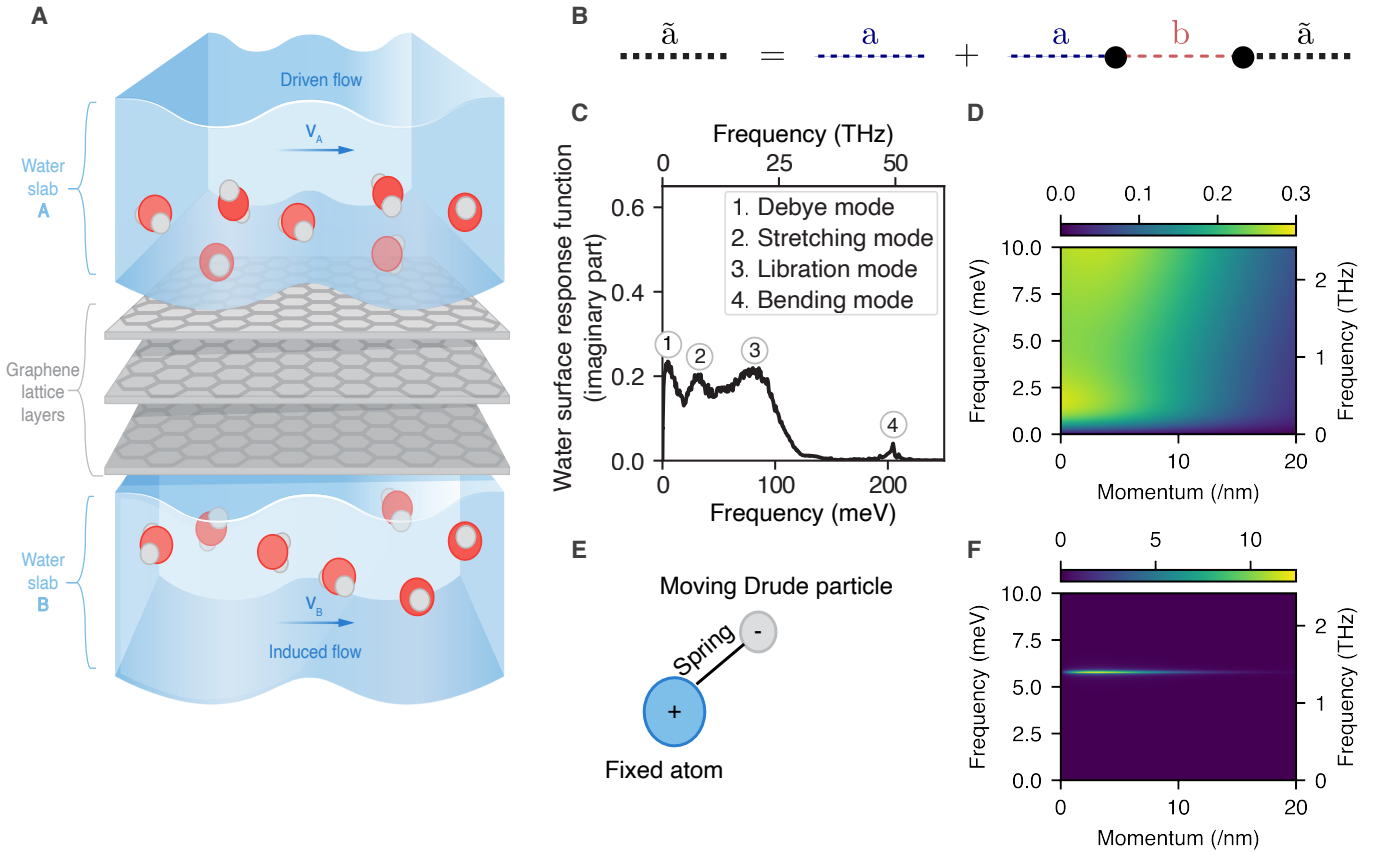


Figure 4. **Model.** (A) Schematic illustrating the system with two liquid films separated by a multi-layer solid. The top liquid is driven out-of-equilibrium and moves at velocity \mathbf{v}_A , transferring momentum to the electrons in the solid via Coulomb drag. After crossing the N layers of solid, this induced excitation further couples to and drags the liquid at the bottom which reaches a velocity \mathbf{v}_B . (B) Dyson equation to compute the Green's function of the layer a renormalized by the layer b. Here, the propagators \tilde{a} represents the renormalized Green's function of layer a, while the propagators a (resp. b) represent the bare Green's functions of layer a (resp. b). (C) Spectrum of water ($\text{Im}[g_w]$) as a function of frequency at momentum $q = 6.7 \text{ nm}^{-1}$, obtained from simulations. The different peaks correspond to different excitation modes (Debye, stretching, libration, bending). (D) Water response function $\text{Im}[g_w]$ as a function of both frequency and momentum using the fit Eq. (36). (E) Schematic representation of the Drude oscillators used to model the electronic modes. An effective electron is attached to an effective nucleus by a spring, generating a plasmon mode. (F) Drude oscillators response function $\text{Im}[g_{Dr}]$ as a function of both frequency and momentum using the formula of Eq. (46). Here, we used $d = 1.675 \text{ \AA}$, a Drude frequency $\omega_p = 1.4 \text{ THz}$ and a relaxation rate $\gamma = 0.1 \text{ THz}$.

where \mathbf{q} is the in-plane momentum and Δz the distance to the interface. Here, the integral over z disappears for a 2d layer. With this definition, the interaction Hamiltonian reduces to

$$\mathcal{H}_{ij}(t) = \int \frac{d\mathbf{q}}{(2\pi)^2} \bar{n}_i(\mathbf{q}, t)^* \bar{n}_j(\mathbf{q}, t) \quad (14)$$

and the linear response of the layer j to a charge fluctuation in the layer i becomes

$$\delta \bar{n}_j(\mathbf{q}, \omega) = -g_j^{R,0}(\mathbf{q}, \omega) \delta \bar{n}_i(\mathbf{q}, \omega) \quad (15)$$

where

$$g_j^{R,0}(\mathbf{r}, t, \mathbf{r}', t') = i\theta(t - t') \langle [\bar{n}_j(\mathbf{r}, t), \bar{n}_j(\mathbf{r}', t')] \rangle \quad (16)$$

is the bare surface response function of the layer j , corresponding to $(-)$ the usual retarded response function for the effective density \bar{n}_j .

Taking into account the self-screening inside the layer j at the RPA level, the surface response function becomes

$$g_j^R(\mathbf{q}, \omega) = \frac{g_j^{R,0}(\mathbf{q}, \omega)}{1 + g_j^{R,0}(\mathbf{q}, \omega)}. \quad (17)$$

To formalise these definitions and develop a rigorous perturbation theory, we introduce the Keldysh formalism.

C. Keldysh formalism

In the following, we use the Keldysh formalism, which is a non-equilibrium perturbation theory. We start by stating some elements of this formalism [22].

We consider particles (bosons or fermions) with creation and annihilation operators $\psi^\dagger(\mathbf{r}, t)$ and $\psi(\mathbf{r}, t)$, respectively. We describe the system's dynamics in terms of three types of real-time Green's functions: the Retarded, Advanced and Keldysh Green's functions, defined, for both bosons and fermions, according to

$$\begin{cases} G^R(\mathbf{r}, t, \mathbf{r}', t') = -i\theta(t - t')\langle[\psi(\mathbf{r}, t), \psi^\dagger(\mathbf{r}', t')]_s\rangle, \\ G^A(\mathbf{r}, t, \mathbf{r}', t') = i\theta(t' - t)\langle[\psi(\mathbf{r}, t), \psi^\dagger(\mathbf{r}', t')]_s\rangle, \\ G^K(\mathbf{r}, t, \mathbf{r}', t') = -i\langle[\psi(\mathbf{r}, t), \psi^\dagger(\mathbf{r}', t')]_{-s}\rangle, \end{cases} \quad (18)$$

where ψ^\dagger and ψ are the particles' creation and annihilation operators, and $[A, B]_\pm = AB \pm BA$, s being $+$ for fermions and $-$ for bosons. In the following, we restrict the discussion to bosons.

The Retarded and Advanced Green's functions contain information on the system's elementary excitations. For free bosons (such as plasmons) with dispersion $\omega_{\mathbf{q}}$ in a translationally-invariant system at equilibrium, the Fourier-transformed Green's functions are

$$G^{R,A} = \frac{\omega_{\mathbf{q}}}{(\omega \pm i0^+)^2 - \omega_{\mathbf{q}}^2}. \quad (19)$$

the Keldysh Green's function contains information on the quasiparticle distribution. At equilibrium, it satisfies the fluctuation-dissipation theorem:

$$G^K(\mathbf{q}, \omega) = 2i \coth\left(\frac{\hbar\omega}{2T}\right) \text{Im} [G^R(\mathbf{q}, \omega)]. \quad (20)$$

Thus, at equilibrium,

$$G^K = (2n_B(\omega) + 1) \times i\pi [\delta(\omega - \omega_{\mathbf{q}}) - \delta(\omega + \omega_{\mathbf{q}})], \quad (21)$$

where we recover the Bose-Einstein distribution $n_B(\omega) = 1/(e^{\hbar\omega/T} - 1)$. The Keldysh Green's functions are therefore the analogues of the occupation distribution functions in the approximate Boltzmann formalism. They will be key in determining the non-equilibrium state of the system.

Here, the system is driven out-of-equilibrium by the flow at velocity \mathbf{v}_A imposed in water slab A. Therefore, the water Green's functions have the form

$$G(\mathbf{r}, t, \mathbf{r}', t') = G_{\text{static}}(\mathbf{r} - \mathbf{v}_A t, t, \mathbf{r}' - \mathbf{v}_A t', t') \quad (22)$$

where G_{static} is the Green's of the static slab of water. Going to Fourier space, this drift becomes a frequency shift:

$$G(\mathbf{q}, \omega) = G_{\text{static}}(\mathbf{q}, \omega - \mathbf{q} \cdot \mathbf{v}_A). \quad (23)$$

Let us outline that these Green's functions no longer fulfill the fluctuation-dissipation theorem: the system is out-of-equilibrium, justifying the use of the Keldysh formalism. Indeed, we now find:

$$G^K(\mathbf{q}, \omega) = 2i \coth\left(\frac{\hbar\omega - \hbar\mathbf{q} \cdot \mathbf{v}_A}{2T}\right) \text{Im} [G^R(\mathbf{q}, \omega)]. \quad (24)$$

Finally, because of the flow tunneling, the induced flow in slab B reaches a steady state velocity \mathbf{v}_B . Similarly, we model this effect by a frequency shift in the Green's function of slab B.

D. Dyson equation

Our task is now to compute the non-equilibrium Green's functions of the layer $i + 1$ in the presence of the perturbation applied by the layer i . This computation is the bosonic analogue to the computation of the electron drag in [23]. In the Keldysh formalism, we consider the matrix Green's function

$$\mathbf{G} = \begin{pmatrix} G^{\text{R}} & G^{\text{K}} \\ 0 & G^{\text{A}} \end{pmatrix}. \quad (25)$$

The perturbation series can be exactly resummed by the non-equilibrium Dyson equation which is represented diagrammatically in Fig. 4b:

$$\tilde{\mathbf{G}}_{i+1} = \mathbf{G}_{i+1} + \mathbf{G}_{i+1} \otimes \mathbf{G}_i \quad (26)$$

where \mathbf{G}_i is the non-interacting Green's function and $\tilde{\mathbf{G}}_i$ the renormalized Green's function. Here, \otimes represents convolution in space and time through the Coulomb potential, as well as matrix multiplication:

$$(\mathbf{A} \otimes \mathbf{B})_{ab}(\mathbf{r}, t, \mathbf{r}', t') = \sum_c \int d\mathbf{r}_A d\mathbf{r}_B dt'' A_{ac}(\mathbf{r}, t, \mathbf{r}_A, t'') V(\mathbf{r}_A - \mathbf{r}_B) B_{cb}(\mathbf{r}_B, t'', \mathbf{r}', t') \quad (27)$$

We assume that the system is translationally invariant parallel to the interface, and that it has reached a steady state: we may then Fourier-transform Eq. (26). If the layer is not 2d, we also need to integrate in the z -direction. Finally, to simplify the computations, we include the Coulombic pre-factor into the Green's functions, leading to introduce the surface response function:

$$g(\mathbf{q}, \omega) = -\frac{e^2}{2\epsilon_0 q} \int dz dz' G(\mathbf{q}, z, z', \omega) e^{-q(|z|+|z'|)} \quad (28)$$

where the integration over z disappears for 2d layers and the origin of z corresponds to the interface.

With the convolutions becoming products in Fourier space, and using that $G^{\text{A}}(\mathbf{q}, \omega) = G^{\text{R}}(\mathbf{q}, \omega)^*$,

$$\tilde{g}_{i+1}^{\text{R}}(\mathbf{q}, \omega) = \frac{g_{i+1}^{\text{R}} - |g_{i+1}^{\text{R}}|^2 (g_i^{\text{R}})^*}{|1 - g_{i+1}^{\text{R}} g_i^{\text{R}}|^2}, \quad (29)$$

$$\tilde{g}_{i+1}^{\text{K}}(\mathbf{q}, \omega) = \frac{g_{i+1}^{\text{K}} + |g_{i+1}^{\text{R}}|^2 g_i^{\text{K}}}{|1 - g_{i+1}^{\text{R}} g_i^{\text{R}}|^2}. \quad (30)$$

For the multi-layer solid with nearest-neighbor interactions, we can compute the surface response function of layer $i + 1$ renormalized by the i previous layers of solid, plus the driven flow, through an iterative procedure. Indeed, we renormalise the response function of layer $i + 1$ by the response function of layer i , itself renormalized by the Green's function of layer $i - 1$, until we reach the driven flow ($i = 0$). As a consequence, we can compute the response function of the N -th layer of solid driven out-of-equilibrium by the driven flow through the $N - 1$ previous layers of solid.

E. Out-of-equilibrium friction forces

We can compute the force between the layer i and the layer $i + 1$ when the system is out-of-equilibrium. This force is formally

$$\mathbf{F}_{i \rightarrow i+1} = \int d\mathbf{r}_i d\mathbf{r}_{i+1} \langle n_i(\mathbf{r}_i, t) V(\mathbf{r}_i - \mathbf{r}_{i+1}) n_{i+1}(\mathbf{r}_{i+1}, t) \rangle, \quad (31)$$

Thus, we need to compute a density-density correlation function, which can be done in Keldysh perturbation theory. Indeed, according to [24], this force writes:

$$\frac{\mathbf{F}_{i \rightarrow i+1}}{\mathcal{A}} = \frac{1}{2} \int \frac{d\mathbf{q} d\omega}{(2\pi)^3} (\hbar \mathbf{q}) \frac{g_i^{\text{R}}(\mathbf{q}, \omega) g_{i+1}^{\text{K}}(\mathbf{q}, \omega) + g_i^{\text{K}}(\mathbf{q}, \omega) g_{i+1}^{\text{A}}(\mathbf{q}, \omega)}{|1 - g_i^{\text{R}}(\mathbf{q}, \omega) g_{i+1}^{\text{R}}(\mathbf{q}, \omega)|^2} \quad (32)$$

Using that $\mathbf{F}_{i \rightarrow i+1} = -\mathbf{F}_{i+1 \rightarrow i}$, we deduce

$$\frac{\mathbf{F}_{i \rightarrow i+1}}{\mathcal{A}} = -\frac{1}{2i} \int \frac{d\mathbf{q} d\omega}{(2\pi)^3} (\hbar \mathbf{q}) \frac{\text{Im} [g_i^{\text{R}}(\mathbf{q}, \omega)] g_{i+1}^{\text{K}}(\mathbf{q}, \omega) - g_i^{\text{K}}(\mathbf{q}, \omega) \text{Im} [g_{i+1}^{\text{R}}(\mathbf{q}, \omega)]}{|1 - g_i^{\text{R}}(\mathbf{q}, \omega) g_{i+1}^{\text{R}}(\mathbf{q}, \omega)|^2} \quad (33)$$

This formula gives the force between two systems interacting with a density-density interaction in general, even when they are out-of-equilibrium. As expected, it has the form of a Landauer formula:

$$\frac{\mathbf{F}_{i \rightarrow i+1}}{\mathcal{A}} = \int \frac{d\mathbf{q}}{(2\pi)^2} (\hbar\mathbf{q}) (\Gamma_{i \rightarrow i+1}(\mathbf{q}) - \Gamma_{i+1 \rightarrow i}(\mathbf{q})) \quad (34)$$

with

$$\Gamma_{i \rightarrow i+1}(\mathbf{q}) = \int \frac{d\omega}{4i\pi} \frac{\text{Im} [g_{i+1}^{\text{R}}(\mathbf{q}, \omega)] g_i^{\text{K}}(\mathbf{q}, \omega)}{|1 - g_i^{\text{R}}(\mathbf{q}, \omega) g_{i+1}^{\text{R}}(\mathbf{q}, \omega)|^2}. \quad (35)$$

Physically, $g_i^{\text{K}}(\mathbf{q}, \omega)$ counts the number of quasi-particles in the layer i at momentum $\hbar\mathbf{q}$ and energy $\hbar\omega$, while $\text{Im} [g_{i+1}^{\text{R}}(\mathbf{q}, \omega)]$ is the "density of states" in the layer $i+1$ at the corresponding momentum and energy to which a quasi-particle may tunnel.

Finally, to compute the friction force of the layer i on the layer $i+1$, we can apply this formula where the Green's function of both layers are renormalized. Because we are computing the force originating from the interaction $\mathcal{H}_{i,i+1}$, the Green's function are to be renormalized by every interaction except this one – otherwise the interaction would be counted twice. Therefore, the layer i 's Green's function is to be renormalized by the layer $i-1$ then $i-2$ until 0 (driven flow) while the layer $(i+1)$'s layer is to be renormalized by the layer $i+2$ then $i+3$ until $N+1$ (induced flow).

IV. MODELS OF WATER AND SOLID

A. Water surface response function and hydrons

The surface response function of water has been studied numerically with Molecular Dynamics (MD) simulations [24–26]. It contains several "hydron" modes (Fig. 4C); at the thermal frequencies that are relevant for quantum friction, those are mainly the Debye mode and the libration mode. Following [24], we describe the water response function by the following formula:

$$g_{\text{w}}^{\text{R}}(\mathbf{q}, \omega) = \frac{1}{2} \left[\frac{\omega_{\text{D},1}}{\omega_{\text{D},1} - i\omega} e^{-q/q_0} + \frac{\omega_{\text{D},2}}{\omega_{\text{D},2} - i\omega} \left(2 - e^{-q/q_0} \right) \right] e^{a+a'(1+(q/b)^\alpha)^{1/\alpha}} \quad (36)$$

where the Debye frequencies are $\omega_{\text{D},1} = 0.36$ THz (*i.e.* $\hbar\omega_{\text{D},1} = 1.5$ meV) and $\omega_{\text{D},2} = 4.8$ THz (*i.e.* $\hbar\omega_{\text{D},2} = 20$ meV), $q_0 = 3.12 \text{ \AA}^{-1}$, $a = 5.16$, $a' = -5.19$, $b = 1.95 \text{ \AA}^{-1}$ and $\alpha = 2$. In particular, the dispersion is weak. This formula is plotted in Fig. 4D.

Within our theoretical framework, we further need to specify the position of a boundary plane separating the water from the solid, which is essentially set by the static water-solid interaction parameters. With the Lennard-Jones parameters of carbon atoms, refs. [1, 24] found that this plane is located at a distance $\delta = 1.3 \text{ \AA}$ from the atomic centers. In our passive wall simulation, agreement with the theory was obtained by setting $\delta = 1 \text{ \AA}$.

B. Drude model of solid

We consider a lattice of Drude oscillators at $z = 0$ whose electron has a mass m_{Dr} and a charge $-Q_{\text{Dr}}$. Each electron is attached to a fixed ion of charge Q_{Dr} through a spring of stiffness K_{Dr} , as sketched in Fig. 4e. We denote \mathbf{r}_k^0 the position of the k -th ion and \mathbf{r}_k the distance between the k -th electron and the k -th ion, so that the harmonic force between them writes

$$\mathbf{F}_{\text{ho}}^k = -K_{\text{Dr}} \mathbf{r}_k. \quad (37)$$

The oscillator is damped by a drag force

$$\mathbf{F}_{\text{th}}^k = -2m_{\text{Dr}} \gamma \partial_t \mathbf{r}_k \quad (38)$$

which corresponds in the simulation to the action of a thermostat through and physically the the effect of phonons and impurities. The only interaction between oscillators are electric. Each oscillator is affected by the local electric potential ϕ . To compute the response function we apply an external electric potential ϕ_{ext} . The local electric field is the sum of an external field and the field induced by the oscillators.

The momentum balance of the k -th oscillator writes

$$m_{\text{Dr}} \partial_t^2 \mathbf{r}_k = -K_{\text{Dr}} \mathbf{r}_k - 2m_{\text{Dr}} \gamma \partial_t \mathbf{r}_k + Q_{\text{Dr}} \nabla \phi(x_k, t). \quad (39)$$

We solve this model in the continuum limit. We denote $\mathbf{u}(\mathbf{r}_k^0, t) = \mathbf{r}_k(t)$ the displacement field and then obtain

$$m_{\text{Dr}} \partial_t^2 \mathbf{u} = -K_{\text{Dr}} \mathbf{u} - 2m_{\text{Dr}} \gamma \partial_t \mathbf{u} + Q_{\text{Dr}} \nabla \phi(x, t). \quad (40)$$

Going to Fourier space we obtain

$$-m_{\text{Dr}} \omega^2 \mathbf{u} = -K_{\text{Dr}} \mathbf{u} + 2im_{\text{Dr}} \gamma \omega \mathbf{u} + iQ_{\text{Dr}} \mathbf{q} \phi(\mathbf{q}, \omega) \quad (41)$$

that is

$$\mathbf{u}(\mathbf{q}, \omega) = \frac{iQ_{\text{Dr}} \mathbf{q}}{K_{\text{Dr}} - m_{\text{Dr}} \omega^2 - 2im_{\text{Dr}} \gamma \omega} \phi(\mathbf{q}, \omega). \quad (42)$$

This displacement field $\mathbf{u}(\mathbf{r}, t)$ generates an electric potential. In the continuum limit, we denote ρ the 2d density of Drude oscillators. At that point, we should distinguish between the longitudinal and transverse modes. For simplicity, we restrict the discussion to the former, the latter being similar. Thus, the induced potential is

$$\phi_{\text{ind}}(\mathbf{r}, z, t) = \int \rho d^2 \mathbf{r}' Q_{\text{Dr}} [V(\mathbf{r} - \mathbf{r}', z) - V(\mathbf{r} - \mathbf{r}' - \mathbf{u}(\mathbf{r}', t), z)] \approx \int \rho d^2 \mathbf{r}' Q_{\text{Dr}} \nabla V(\mathbf{r} - \mathbf{r}', z) \cdot \mathbf{u}(\mathbf{r}', t) \quad (43)$$

where V is the Coulomb potential. Going to Fourier space, we obtain,

$$\phi_{\text{ind}}(\mathbf{q}, z, \omega) = \frac{\rho Q_{\text{Dr}}}{2\epsilon_0 q} e^{-q|z|} i\mathbf{q} \cdot \mathbf{u}(\mathbf{q}, \omega) = -\frac{\rho Q_{\text{Dr}}^2}{2\epsilon_0 m_{\text{Dr}}} \frac{q e^{-q|z|}}{\frac{K_{\text{Dr}}}{m_{\text{Dr}}} - \omega^2 - 2i\gamma\omega} \phi(q, \omega) \quad (44)$$

where $n_{\text{Dr}}(\mathbf{r}, t) = \rho Q_{\text{Dr}} \nabla \cdot \mathbf{u}(\mathbf{r}, t)$ is the charge density in the material. Denoting $\omega_p = \sqrt{K_{\text{Dr}}/m_{\text{Dr}}}$ the Drude frequency and $\ell_p = \rho Q_{\text{Dr}}^2 / (2\epsilon_0 K_{\text{Dr}})$ a length, we have

$$g_{\text{Dr}}^{\text{R}}(\mathbf{q}, \omega) = \frac{\omega_p^2 \ell_p q}{\omega_p^2 - \omega^2 - 2i\gamma\omega}, \quad \phi_{\text{ind}}(\mathbf{q}, z, \omega) = -g_{\text{Dr}}^{\text{R}}(\mathbf{q}, \omega) e^{-q|z|} \phi(q, \omega). \quad (45)$$

At this stage, we have not taken into account the Coulomb interaction between the Drude oscillators. Including them would lead to a dispersion of the Drude frequency. However, the simulations show that this dispersion is negligible, and we therefore use the non-interacting expression in the following.

Since we always consider interactions between layers separated by a distance d_0 , it will be convenient to redefine the surface response function according to

$$g_{\text{Dr}}^{\text{R}}(\mathbf{q}, \omega) = \frac{\omega_p^2 \ell_p q e^{-2qd_0}}{\omega_p^2 - \omega^2 - 2i\gamma\omega}, \quad (46)$$

and then carry out the computations as if there was no separation between the layers. We use we use $d_0 = 1.675 \text{ \AA}$ (half the distance between two graphitic layers) when computing the response to another solid layer, and $d_0 = \delta$ when computing the response to a water slab. Eq. (46) is plotted in Fig. 4F.

C. Effect of phonons

The effect of phonons on flow tunneling was previously studied by Andreev and Meierovitch [27] and shown to be negligible for all practical purposes. In their model, the Authors consider the flow induced throughout a dissipation-less solid induced by a Poiseuille flow in a channel of height a . According to their results, the induced velocity writes:

$$\frac{v_B}{v_A} = \zeta \left(\frac{3}{2} \right) \frac{T}{4\eta} \sqrt{\frac{\rho_\ell^5 c_\ell^3}{\pi^5 \rho_s^2 y^3 a c_s^T}} \Phi \left(\frac{c_\ell}{c_s^T}, \frac{c_s^L}{c_s^T} \right) \quad (47)$$

where ζ is the Riemann-function and Φ is a dimensionless pre-factor defined in [27] and typically ranging between 10^{-2} and 1. Here, ρ_ℓ and ρ_s are the densities of the liquid and the solid respectively, c_ℓ is the velocity of sound in the liquid and c_s^L and c_s^T the velocity of longitudinal/transverse sound in the solid. Finally, $y = 4\eta/3 + \hat{\eta} + \kappa(c_p - c_v)/c_p c_v$ is a parameter of the liquid with κ the thermal conductivity c_p and c_v the specific heats per unit mass, and η and $\hat{\eta}$ the first and second viscosities.

Notably, the efficiency of the phonon-mediated flow tunneling scales with $1/\sqrt{a}$. Thus, the flow tunneling is larger when the driving flow is confined. Physically, this comes from the stronger shear in the confined Poiseuille flow which produces more phonons. However, the model of [27] neglects slippage and then the coefficient a in Eq. (47) should be replaced by the slip length at strongest confinements. Finally, applying Eq. (47) to nano-confined liquids separated by a graphite wall, one finds a tunneling efficiency $v_B/v_A \sim 10^{-5}$, which is negligible.

V. FLOW TUNNELING

A. Simplified expression of fluctuation-induced friction

Before considering the flow tunneling geometry, we first provide a simplified expression of the solid-liquid quantum friction force, starting from Eq. (34). We assume the liquid, labeled w , to flow at velocity \mathbf{v} while the solid, labelled e , is at equilibrium. Then,

$$g_w^K(\mathbf{q}, \omega) = \coth \left(\frac{\hbar\omega - \hbar\mathbf{q}\mathbf{v}}{2T} \right) \text{Im} [g_w^R(q, \omega)], \quad g_e^K(q, \omega) = \coth \left(\frac{\hbar\omega}{2T} \right) \text{Im} [g_e^R(q, \omega)]. \quad (48)$$

Thus, to first order in \mathbf{v} , and after carrying out the angular integration, Eq. (34) becomes

$$\frac{\mathbf{F}_{e \rightarrow w}}{\mathcal{A}} = -\frac{\hbar^2}{16\pi^2 T} \mathbf{v} \int_0^\infty dq q^3 \int_{-\infty}^\infty d\omega \frac{1}{\sinh^2 \left(\frac{\hbar\omega}{2T} \right)} \frac{\text{Im} [g_w^R(q, \omega)] \text{Im} [g_e^R(q, \omega)]}{|1 - g_w^R(q, \omega)g_e^R(q, \omega)|^2}, \quad (49)$$

which is the result of [24].

For the Drude solid in the limit of small damping ($\gamma \rightarrow 0$), the surface response function becomes

$$\text{Im} [g_{\text{Dr}}^R(q, \omega)] = \frac{\pi}{2} \omega \delta(\omega \pm \omega_p) \times q \ell_p e^{-2qd_0}. \quad (50)$$

Here, $d_0 = \delta = 1.3 \text{ \AA}$ is the distance between the atomic centers and the imaginary plane separating water from the solid (see Sec. IV A). Further neglecting the denominator (that corresponds to higher order corrections) in Eq. (49) and approximating $\hbar\omega_p \ll T$ in the integrand, the quantum friction coefficient becomes

$$\lambda_{\text{qf}} = \frac{T \ell_p}{4\pi} \int_0^\infty dq q^4 e^{-2qd_0} \times \frac{1}{\omega_p} \text{Im} [g_w^R(q, \omega_p)] \quad (51)$$

We may further neglect the momentum dependence of the water surface response function and approximate it as a single Debye peak, that is

$$\text{Im} [g_w^R(\mathbf{q}, \omega)] \approx \alpha_w \frac{\omega \omega_0}{\omega_0^2 + \omega^2}, \quad (52)$$

where α_w is an effective amplitude of the Debye peak at around $q \approx 1/d_0$. Then, the quantum friction coefficient writes

$$\lambda_{\text{qf}} \approx \frac{3}{16\pi} \frac{T \ell_p \alpha_w}{d_0^5} \frac{\omega_0}{\omega_0^2 + \omega_p^2} \approx \frac{10^5 \text{ N.s/m}^3}{1 + (\omega_p/\omega_0)^2}. \quad (53)$$

Thus, when the Drude plasmon frequency is larger than the Debye frequency, the quantum friction coefficient scales with $\lambda_{\text{qf}} \propto 1/\omega_p^2$, while the coefficient goes to a constant when the Drude plasmon frequency becomes small compared to the Debye frequency. This simple formula provides a good fit to the full result of Eq. (49), with parameters $\alpha_w \approx 2 \cdot 10^{-2}$ and the effective Debye frequency $\omega_0 \approx 0.3 \text{ THz}$ (see Fig. 6A).

Here, we discussed the case of a single interface between a slab of water and a Drude layer. For the scenario of flow tunneling with N layers of solid before another slab of water at equilibrium, the quantum friction coefficient can also be computed and corresponds to the blue curves in 6A. When $N = 1$, the presence of water on the other side of the solid layer increases the quantum friction, as it brings about additional charge fluctuations. For larger values of N , the effect of the second water slab becomes negligible and the quantum friction is almost identical to the single layer case.

B. Flow tunneling through a passive solid

We start with the case of an inert solid. According to Eq. (34) the force applied by water slab A on water slab B is

$$\frac{\mathbf{F}_{\text{hh}}}{\mathcal{A}} = \int \frac{d\mathbf{q}}{(2\pi)^2} (\hbar\mathbf{q}) (\Gamma_{A \rightarrow B}(\mathbf{q}) - \Gamma_{B \rightarrow A}(\mathbf{q})) \quad (54)$$

with

$$\Gamma_{a \rightarrow b}(\mathbf{q}) = \int \frac{d\omega}{4i\pi} \frac{g_w^K(\mathbf{q}, \omega - \mathbf{q} \cdot \mathbf{v}_a) \text{Im} [g_w^R(\mathbf{q}, \omega - \mathbf{q} \cdot \mathbf{v}_b)] e^{-2qd}}{|1 - g_w^R(\mathbf{q}, \omega - \mathbf{q} \cdot \mathbf{v}_a)g_w^R(\mathbf{q}, \omega - \mathbf{q} \cdot \mathbf{v}_b)|^2} \quad (55)$$

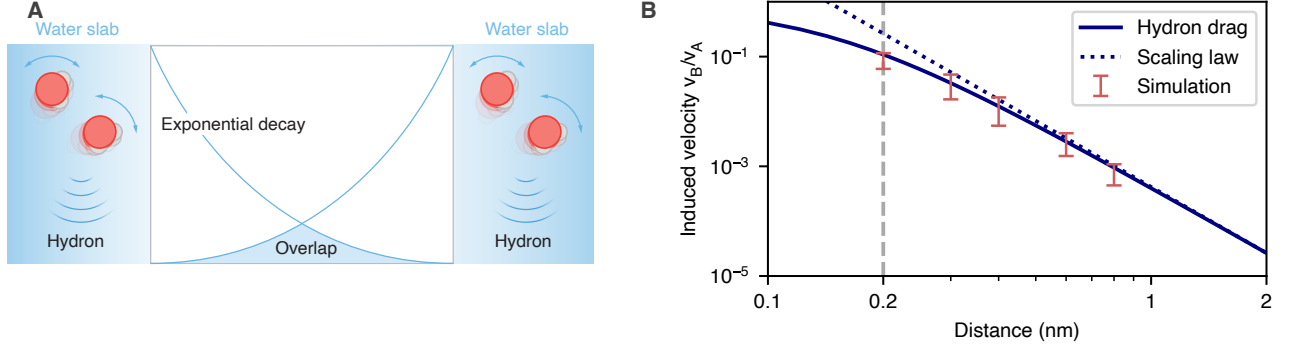


Figure 5. **Flow tunneling through an inert solid.** (A) Schematic of the tunneling of elementary excitations (hydrons) between two water slabs. Tunneling occurs when the associated Coulomb potentials overlap. (B) Ratio of the tunneling-induced velocity v_B and imposed velocity v_A versus thickness of the inert solid d , assumed to have a classical (roughness-induced) friction coefficient $\lambda_{cl} \approx 2.1 \cdot 10^4 \text{ N} \cdot \text{s} \cdot \text{m}^{-3}$. The vertical dashed line indicates the value of d below which the separation between the water slabs becomes ill-defined. Error bars represent the mean-squared error over simulations.

where g_w is the equilibrium water surface response function and d is the thickness of the solid. Shifting the frequencies and using the fluctuation-dissipation theorem (Eq. (20)) leads to

$$\Gamma_{a \rightarrow b}(\mathbf{q}) = \int \frac{d\omega}{2\pi} (2n_B(\omega - \mathbf{q} \cdot \mathbf{v}_a) + 1) \frac{\text{Im} [g_w^R(\mathbf{q}, \omega - \mathbf{q} \cdot \mathbf{v}_a)] \text{Im} [g_w^R(\mathbf{q}, \omega - \mathbf{q} \cdot \mathbf{v}_b)] e^{-2qd}}{|1 - g_w^R(\mathbf{q}, \omega - \mathbf{q} \cdot \mathbf{v}_a) g_w^R(\mathbf{q}, \omega - \mathbf{q} \cdot \mathbf{v}_b) e^{-2qd}|^2} \quad (56)$$

Here, $f_{\mathbf{q}}^a(E) = n_B(E/\hbar - \mathbf{q} \cdot \mathbf{v}_a)$ is the average number of hydrons of wavevector \mathbf{q} and energy E . Using that $\text{Re} [g_w^R(\mathbf{q}, \omega)]$ is symmetric in ω and $\text{Im} [g_w^R(\mathbf{q}, \omega)]$ is antisymmetric in ω , Eq. (54) becomes, to first order in velocities:

$$\frac{\mathbf{F}_{hh}}{\mathcal{A}} = \frac{1}{2\pi\hbar} \int dE \int \frac{d\mathbf{q}}{(2\pi)^2} (\hbar\mathbf{q}) (f_{\mathbf{q}}^T(E) - f_{\mathbf{q}}^B(E)) \mathcal{T}_{\mathbf{q}}(E) \quad (57)$$

where

$$\mathcal{T}_{\mathbf{q}}(\hbar\omega) = 2 \frac{\text{Im} [g_w^R(\mathbf{q}, \omega)]^2 e^{-2qd}}{|1 - g_w^R(\mathbf{q}, \omega)^2 e^{-2qd}|^2} \quad (58)$$

is the dimensionless transmission coefficient. We thus recover on rigorous grounds the Landauer-like formula that was suggested in the main text.

To obtain the scaling of the driving force with d , we make the same approximations as in the previous subsection. Namely, we neglect the denominator of Eq. (58), the momentum dependence of the water surface response function and approximate

$$\text{Im} [g_w^R(\mathbf{q}, \omega)] \approx \alpha_w \frac{\omega_0 \omega}{\omega_0^2 + \omega^2} \quad (59)$$

where $\omega_0 \approx 0.3 \text{ THz} \ll T/\hbar$ is the effective Debye frequency and α_w an amplitude factor. Still to first order in velocities, we then obtain

$$\frac{\mathbf{F}_{hh}}{\mathcal{A}} \approx \frac{\alpha_w T \Delta \mathbf{v}}{2\pi^2} \int_0^\infty dq q^3 e^{-2qd} \int_0^\infty d\omega \frac{\omega_0^2}{(\omega_0^2 + \omega^2)^2} = \frac{3}{64\pi^2} \frac{\alpha_w T}{\omega_0 d^4} \Delta \mathbf{v} \propto \frac{1}{d^4} \quad (60)$$

where $\Delta \mathbf{v} = \mathbf{v}_A - \mathbf{v}_B$. We thus recover from rigorous theory the $1/d^4$ scaling obtained from the simple model in the main text.

We may thus introduce the hydron-hydron friction coefficient as $\lambda_{hh} = \mathbf{F}_{hh}/(\mathcal{A}\Delta \mathbf{v})$. \mathbf{F}_{hh} is the driving force for the flow tunneling effect: it induces the flow of fluid B in response to the flow of fluid A . In the steady state, \mathbf{F}_{hh} is balanced by the classical (roughness-induced) friction $\mathbf{F}_{cl} = -\lambda_{cl} \mathcal{A} \mathbf{v}_B$ exerted on fluid B by the solid wall, so that

$$v_B = \frac{\lambda_{hh}}{\lambda_{hh} + \lambda_{cl}} v_A. \quad (61)$$

This result is compared to MD simulations in Fig. 5. When λ_{hh} is computed with Eq. (57), we obtain quantitative agreement with the simulations; Eq. (60) matches the long-distance scaling.

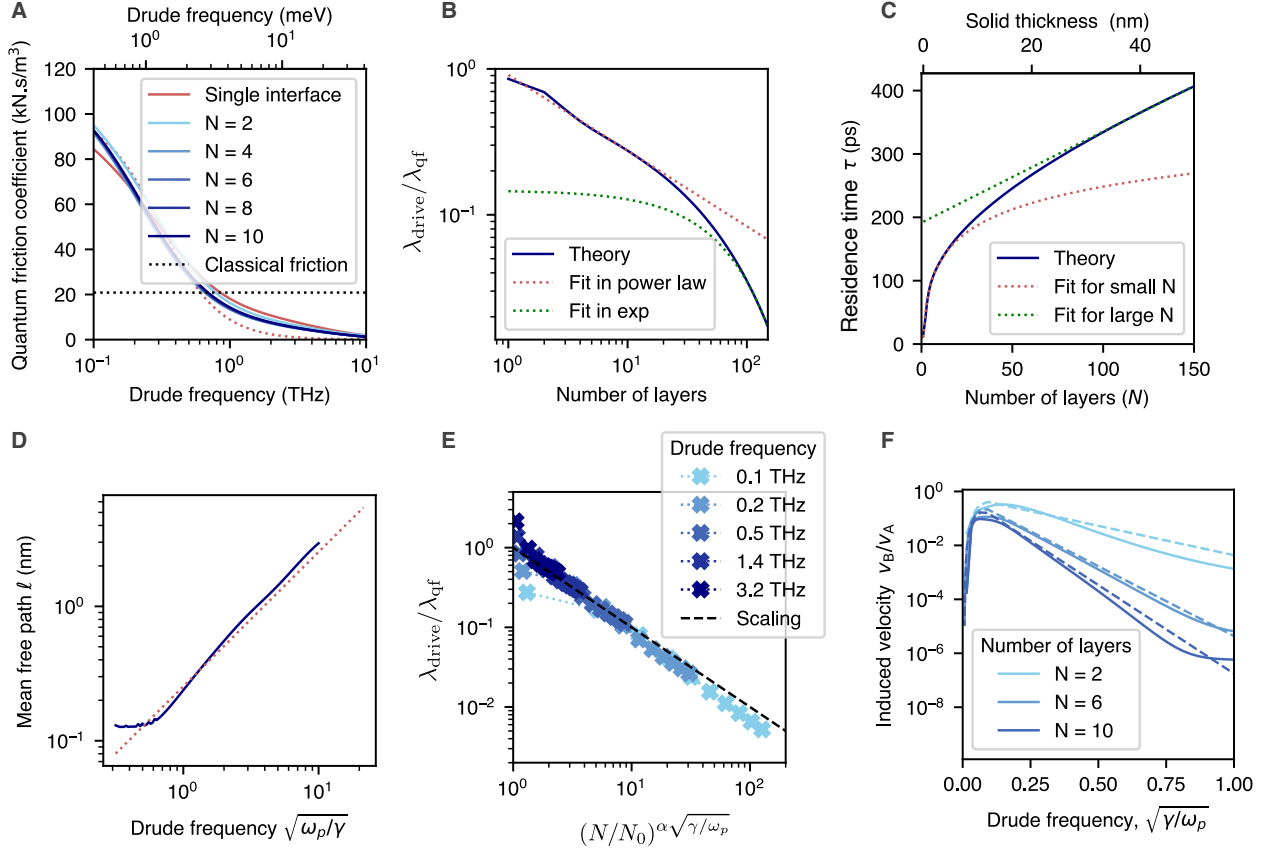


Figure 6. **Scaling regimes.** (A) Quantum friction coefficient of a water slab on a layer Drude oscillators (in red) and on N layers of Drude oscillators with another slab of water behind. The red dashed line corresponds to the simple estimate of quantum friction Eq. (53). The black dashed line corresponds to the classical friction. Here, the quantum friction is plotted as a function of the Drude frequency ω_p with a relaxation rate of $\gamma = 10^{-2}$ THz. (B) Ratio $\lambda_{\text{drive}}/\lambda_{\text{qf}}$ as a function of the number of layers with a Drude frequency $\omega_p = 1.4$ THz and a relaxation rate of $\gamma = 10^{-2}$ THz. The dashed red curve is an algebraic fit and the dashed green curve is an exponential fit. (C) Residence time τ as defined in Eq. (65) as a function of the number of layers with a Drude frequency $\omega_p = 1.4$ THz and a relaxation rate of $\gamma = 10^{-2}$ THz. The dashed red curve is a fit in $\log N$ valid at small distances (algebraic regime) while the dashed green curve is a linear fit valid at large distances (exponential regime). (D) Hydron mean free path ℓ , as defined in Eq. (66), versus rescaled Drude frequency $\sqrt{\omega_p/\gamma}$ at $\gamma = 10^{-1}$ THz. The dashed line is $\ell = \ell_0 \sqrt{\omega_p/\gamma}$. (E) Ratio $\lambda_{\text{drive}}/\lambda_{\text{qf}}$ versus rescaled number of layers. At not too large N , the all values of ω_p collapse onto the scaling expression of Eq. (68). We have fixed $\gamma = 10^{-2}$ THz. (F) Tunneling efficiency v_B/v_A versus rescaled Drude frequency $\sqrt{\gamma/\omega_p}$. The dashed lines correspond to Eq. (67). We have fixed $\gamma = 10^{-2}$ THz.

C. Flow tunneling through an active solid

Let us now study the flow tunneling in presence of the solid's excitation modes. For this, we compute the out-of-equilibrium friction force between the solid and the induced flow. To first order in velocities, this friction force is of the form

$$\frac{\mathbf{F}_{N \rightarrow B}}{\mathcal{A}} = \lambda_{\text{drive}} \mathbf{v}_A - \lambda_{\text{qf}} \mathbf{v}_B \quad (62)$$

where the first term corresponds to the driving force due to the imposed flow and the second term corresponds to dissipation due to the quantum friction experienced by the induced fluid flowing at velocity \mathbf{v}_B . Let us stress, however, that these two terms split only to first order in velocities, and they both originate in the same fluctuating Coulomb interactions between the liquid and the solid.

In practice $\mathbf{F}_{N \rightarrow B}$ is computed by numerically carrying out the integrals in Eq. (34) (with surface response functions renormalized through the iterative procedure described in Sec. III D), for imposed values of \mathbf{v}_A and \mathbf{v}_B in the linear response regime. By evaluating $\mathbf{F}_{N \rightarrow B}$ for two pairs of velocities ($\mathbf{v}_A, \mathbf{v}_B^1$) and ($\mathbf{v}_A, \mathbf{v}_B^2$), we obtain the friction coefficients λ_{drive} and λ_{qf} .

In addition to the flow tunneling driving force $\mathbf{F}_{N \rightarrow B}$, fluid B is subject to classical friction on the N^{th} solid layer ($\mathbf{F}_{\text{cl}} = -\lambda_{\text{cl}}\mathcal{A}\mathbf{v}_B$), and to the direct friction force with fluid A if the solid is very thin ($\mathbf{F}_{\text{hh}} = \lambda_{\text{hh}}\mathcal{A}(\mathbf{v}_A - \mathbf{v}_B)$). Finally, imposing momentum balance in the steady state yields the magnitude of flow tunneling:

$$\mathbf{v}_B = \frac{\lambda_{\text{drive}} + \lambda_{\text{hh}}}{\lambda_{\text{qf}} + \lambda_{\text{cl}} + \lambda_{\text{hh}}}\mathbf{v}_A. \quad (63)$$

For $N > 1$, we may neglect λ_{hh} , so that

$$\frac{v_B}{v_A} \approx \frac{\lambda_{\text{qf}}}{\lambda_{\text{qf}} + \lambda_{\text{cl}}} \frac{\lambda_{\text{drive}}}{\lambda_{\text{qf}}}. \quad (64)$$

D. Scaling regimes of the tunneling efficiency

The dependence of the tunneling efficiency on the number of solid layers N is contained in the dimensionless ratio $\lambda_{\text{drive}}/\lambda_{\text{qf}}$. This ratio is plotted as a function of N (for representative values of ω_p and γ) in Fig. 6B. It displays a crossover from a power law scaling at small N to an exponential scaling at large N . As in the main text, we may define a "hydron residence time"

$$\tau = -\frac{\log(\lambda_{\text{drive}}/\lambda_{\text{qf}})}{\gamma}. \quad (65)$$

The exponential scaling for $\lambda_{\text{drive}}/\lambda_{\text{qf}}$ translates into a linear scaling for τ (Fig. 6C), anticipated on qualitative grounds in the main text:

$$\tau \approx \tau_{\text{sl}} + \frac{Nd_0}{\ell} = \tau_{\text{sl}} + \frac{d}{\ell}, \quad (66)$$

which defines the hydron mean free path $\ell(\omega_p, \gamma)$. We find numerically that the mean free path scales as $\ell \approx \ell_0 \sqrt{\frac{\omega_p}{\gamma}}$ with $\ell_0 \approx 0.26$ nm (Fig. 6D). Altogether, the tunneling efficiency in this regime is given by

$$\frac{v_B}{v_A} \approx \frac{\lambda_{\text{qf}}}{\lambda_{\text{qf}} + \lambda_{\text{cl}}} e^{-\gamma\tau_{\text{sl}} + (d/\ell_0)\sqrt{\gamma/\omega_p}}. \quad (67)$$

The power law regime is described by

$$\frac{\lambda_{\text{drive}}}{\lambda_{\text{qf}}} \approx \left(\frac{N_0}{N}\right)^{\alpha\sqrt{\gamma/\omega_p}} \quad (68)$$

with $N_0 \approx 0.84$ and $\alpha \approx 6.2$. Fig. 6E shows the collapse of $\lambda_{\text{drive}}/\lambda_{\text{qf}}$ on this scaling form for a range of values of ω_p , at small enough N . Nevertheless, we find that, even at not too large N , Eq. (67) still provides a reasonable description of the tunneling efficiency v_B/v_A , as shown in Fig. 6F. Eq. (67) may therefore be used to qualitatively discuss the influence of the parameters N , γ and ω_p on the tunneling efficiency.

-
- [1] Anna T. Bui, Fabian L. Thiemann, Angelos Michaelides, and Stephen J. Cox, "Classical quantum friction at water-carbon interfaces," *Nano Letters* **23**, 580–587 (2023).
 - [2] Aidan P. Thompson, H. Metin Aktulga, Richard Berger, Dan S. Bolintineanu, W. Michael Brown, Paul S. Crozier, Pieter J. in 't Veld, Axel Kohlmeyer, Stan G. Moore, Trung Dac Nguyen, Ray Shan, Mark J. Stevens, Julien Tranchida, Christian Trott, and Steven J. Plimpton, "LAMMPS - a flexible simulation tool for particle-based materials modeling at the atomic, meso, and continuum scales," *Computer Physics Communications* **271**, 108171 (2022).
 - [3] H. J. C. Berendsen, J. R. Grigera, and T. P. Straatsma, "The missing term in effective pair potentials," *The Journal of Physical Chemistry* **91**, 6269–6271 (1987).
 - [4] Hans C. Andersen, "Rattle: A "velocity" version of the shake algorithm for molecular dynamics calculations," *Journal of Computational Physics* **52**, 24–34 (1983).
 - [5] R.W. Hockney and J.W. Eastwood, *Computer Simulation Using Particles* (Adam-Hilger, 1988).
 - [6] Jiri Kolafa and John W. Perram, "Cutoff errors in the ewald summation formulae for point charge systems," *Molecular Simulation* **9**, 351–368 (1992).

- [7] In-Chul Yeh and Max L. Berkowitz, "Ewald summation for systems with slab geometry," *The Journal of Chemical Physics* **111**, 3155–3162 (1999).
- [8] Wataru Shinoda, Motoyuki Shiga, and Masuhiro Mikami, "Rapid estimation of elastic constants by molecular dynamics simulation under constant stress," *Phys. Rev. B* **69**, 134103 (2004).
- [9] Mark E Tuckerman, José Alejandro, Roberto López-Rendón, Andrea L Jochim, and Glenn J Martyna, "A liouville-operator derived measure-preserving integrator for molecular dynamics simulations in the isothermal–isobaric ensemble," *Journal of Physics A: Mathematical and General* **39**, 5629–5651 (2006).
- [10] Lydéric Bocquet and Jean-Louis Barrat, "Hydrodynamic boundary conditions, correlation functions, and kubo relations for confined fluids," *Phys. Rev. E* **49**, 3079–3092 (1994).
- [11] Lydéric Bocquet, Jean-Pierre Hansen, and Jaroslaw Piasecki, "Friction tensor for a pair of brownian particles: Spurious finite-size effects and molecular dynamics estimates," *Journal of Statistical Physics* **89**, 321–346 (1997).
- [12] Pep Español, J. A. de la Torre, and D. Duque-Zumajo, "Solution to the plateau problem in the Green–Kubo formula," *Phys. Rev. E* **99**, 022126 (2019).
- [13] Kerstin Falk, Felix Sedlmeier, Laurent Joly, Roland R. Netz, and Lydéric Bocquet, "Ultralow liquid/solid friction in carbon nanotubes: Comprehensive theory for alcohols, alkanes, OMCTS, and water," *Langmuir* **28**, 14261–14272 (2012).
- [14] Gabriele Tocci, Laurent Joly, and Angelos Michaelides, "Friction of water on graphene and hexagonal boron nitride from ab initio methods: Very different slippage despite very similar interface structures," *Nano Letters* **14**, 6872–6877 (2014).
- [15] Anthony R. Poggioli and David T. Limmer, "Distinct chemistries explain decoupling of slip and wettability in atomically smooth aqueous interfaces," *The Journal of Physical Chemistry Letters* **12**, 9060–9067 (2021).
- [16] T. Werder, J. H. Walther, R. L. Jaffe, T. Halicioglu, and P. Koumoutsakos, "On the water–carbon interaction for use in molecular dynamics simulations of graphite and carbon nanotubes," *The Journal of Physical Chemistry B* **107**, 1345–1352 (2003).
- [17] Guillaume Lamoureux and Benoit Roux, "Modeling induced polarization with classical Drude oscillators: Theory and molecular dynamics simulation algorithm," *The Journal of Chemical Physics* **119**, 3025–3039 (2003).
- [18] Rahul Prasanna Misra and Daniel Blankschtein, "Insights on the role of many-body polarization effects in the wetting of graphitic surfaces by water," *The Journal of Physical Chemistry C* **121**, 28166–28179 (2017).
- [19] Alain Dequidt, Julien Devémy, and Agílio A. H. Prádua, "Thermalized Drude oscillators with the LAMMPS molecular dynamics simulator," *Journal of Chemical Information and Modeling* **56**, 260–268 (2016).
- [20] B. T. Thole, "Molecular polarizabilities calculated with a modified dipole interaction," *Chemical Physics* **59**, 341–350 (1981).
- [21] Abraham. Savitzky and M. J. E. Golay, "Smoothing and differentiation of data by simplified least squares procedures." *Analytical Chemistry* **36**, 1627–1639 (1964).
- [22] Jorgen Rammer, *Quantum Field Theory of Non-equilibrium States* (Cambridge University Press, 2007).
- [23] Baptiste Coquinot, Lydéric Bocquet, and Nikita Kavokine, "Quantum feedback at the solid-liquid interface: Flow-induced electronic current and its negative contribution to friction," *Phys. Rev. X* **13**, 011019 (2023).
- [24] Nikita Kavokine, Marie-Laure Bocquet, and Lydéric Bocquet, "Fluctuation-induced quantum friction in nanoscale water flows," *Nature* **602**, 84–90 (2022).
- [25] Douwe Jan Bonthuis, Stephan Gekle, and Roland R. Netz, "Profile of the Static Permittivity Tensor of Water at Interfaces: Consequences for Capacitance, Hydration Interaction and Ion Adsorption," *Langmuir* **28**, 7679–7694 (2012).
- [26] Baptiste Coquinot, Maximilian Becker, Roland R. Netz, Lydéric Bocquet, and Nikita Kavokine, "Collective modes and quantum effects in two-dimensional nanofluidic channels," *Faraday Discussions* (2023), 10.1039/D3FD00115F.
- [27] A. F. Andreev and A. E. Meierovich, "Dragging of a liquid by a liquid through a stationary solid wall," *JETP Lett.* **15** (1971).